



S-Nitrosylation of the histone deacetylase HDA19 stimulates its activity to enhance plant stress tolerance in Arabidopsis

Yu Zheng, Zhenting Li, Xiaoyun Cui, Zheng Yang, Chun Bao, Lei Pan,
Xiaoyun Liu, Gilles Chatel-innocenti, H  l  ne Vanacker, Graham Noctor, et al.

► To cite this version:

Yu Zheng, Zhenting Li, Xiaoyun Cui, Zheng Yang, Chun Bao, et al.. S-Nitrosylation of the histone deacetylase HDA19 stimulates its activity to enhance plant stress tolerance in Arabidopsis. *Plant Journal*, 2023, 114 (4), pp.836-854. 10.1111/tpj.16174 . hal-04304589v2

HAL Id: hal-04304589


<https://hal.science/hal-04304589v2>

Submitted on 28 Nov 2023

HAL is a multi-disciplinary open access archive for the deposit and dissemination of scientific research documents, whether they are published or not. The documents may come from teaching and research institutions in France or abroad, or from public or private research centers.

L'archive ouverte pluridisciplinaire **HAL**, est destinée au dépôt et à la diffusion de documents scientifiques de niveau recherche, publiés ou non, émanant des établissements d'enseignement et de recherche français ou étrangers, des laboratoires publics ou privés.

S-Nitrosylation of the histone deacetylase HDA19 stimulates its activity to enhance plant stress tolerance in Arabidopsis

Yu Zheng^{1,2,*} , **Zhenting Li**^{1,†}, **Xiaoyun Cui**², **Zheng Yang**², **Chun Bao**¹, **Lei Pan**¹, **Xiaoyun Liu**¹, **Gilles Chatel-Innocenti**², **Hélène Vanacker**², **Graham Noctor**², **Avilien Dard**³, **Jean-Philippe Reichheld**³ , **Emmanuelle Issakidis-Bourguet**² and **Dao-Xiu Zhou**^{2,*}

¹Hubei Province Research Center of Legume Plants, School of Life Science and Institute for Interdisciplinary Research, Jiangnan University, Wuhan 430056, China.

²*Institute of Plant Sciences Paris-Saclay, CNRS, INRA, Université Paris-Saclay, 91405, Orsay, France, and*

³Laboratoire Génome et Développement des Plantes, CNRS, Université Perpignan Via Domitia, 66860, Perpignan, France

Received 12 December 2022; revised 6 February 2023; accepted 26 February 2023.

*For correspondence (e-mail zhengyu@ihun.edu.cn; dao-xiu.zhou@universite-paris-saclay.fr).

[†]These authors are co-first authors.

SUMMARY

Arabidopsis histone deacetylase HDA19 is required for gene expression programs of a large spectrum of plant developmental and stress-responsive pathways. How this enzyme senses cellular environment to control its activity remains unclear. In this work, we show that HDA19 is post-translationally modified by S-nitrosylation at 4 Cysteine (Cys) residues. HDA19 S-nitrosylation depends on the cellular nitric oxide level, which is enhanced under oxidative stress. We find that HDA19 is required for cellular redox homeostasis and plant tolerance to oxidative stress, which in turn stimulates its nuclear enrichment, S-nitrosylation and epigenetic functions including binding to genomic targets, histone deacetylation and gene repression. The Cys137 of the protein is involved in basal and stress-induced S-nitrosylation, and is required for HDA19 functions in developmental, stress-responsive and epigenetic controls. Together, these results indicate that S-nitrosylation regulates HDA19 activity and is a mechanism of redox-sensing for chromatin regulation of plant tolerance to stress.

Keywords: S-nitrosylation, HDA19, oxidative stress, post-translational modifications, epigenetics.

INTRODUCTION

Histone acetylation/deacetylation is an important epigenetic modification for chromatin remodeling and gene expression. The dynamic equilibrium of histone acetylation is regulated by histone acetyltransferases (HATs) and histone deacetylases (HDACs; Mikkelsen et al., 2007; Ueda et al., 2017; Yuan et al., 2013). In Arabidopsis, there are 12 HDACs belonging to the reduced potassium dependency 3 (RPD3/HDA1) family, four to the histone deacetylase 2 (HD2) group, and two to the silent information regulator 2 (SIR2) or sirutin proteins (Alinsug et al., 2009; Pandey et al., 2002). Many studies have shown that HDA19, a RPD3 family member, plays an essential role in plant growth and development, including meristem function; morphology of seedling, leaf and floral organs; flowering time; fertility; seed maturation and germination (Benhamed et al., 2006; Krogan et al., 2012; Long et al., 2006; Ryu et al., 2014; Tanaka et al., 2008; Tian et al., 2003; Zhou et al., 2013). In addition, HDA19 is also

implicated in plant defense and response to environmental stresses (Gao et al., 2015; Gorham et al., 2018; Pi et al., 2015; Ryu et al., 2014; Shen et al., 2019; Song et al., 2005; Ueda et al., 2018; Zhou et al., 2005). *HDA19* overexpression upregulates several ethylene/jasmonic acid-induced genes and enhances resistance to a fungal pathogen (Zhou et al., 2005), while its mutation de-represses salicylic acid (SA) biosynthesis and SA-mediated defense gene expression and responses (Jang et al., 2011; Kim et al., 2008). *HDA19* is also required for plant response to abiotic stresses such as drought, salt, high temperature and abscisic acid signaling (Mehdi et al., 2016; Perrella et al., 2013; Ryu et al., 2014; Song et al., 2005; Ueda et al., 2017). However, recent data indicate that compared with other HDAC members (i.e. *HDA5/14/15/18*), *HDA19* regulates different pathways of plant response to salt stress and high temperature (Shen et al., 2019; Ueda et al., 2018). *HDA19* is reported to form transcriptional repressive complexes with various co-repressors such as *TOPLESS*

(TPL), LEUNIG, SWI-INDEPENDENT3 (SIN3) and SIN3-LIKE (SNL) proteins, and to interact with transcription factors such as AP2/EREBP, BES1, SCR-like15, WOX5 and others to repress genes involved in different developmental and stress-responsive pathways through histone deacetylation (Gao et al., 2015; Gonzalez et al., 2007; Krogan et al., 2012; Long et al., 2006; Mehdi et al., 2016; Pi et al., 2015; Ryu et al., 2014; Song et al., 2005; Wang et al., 2013). The versatile function of HDA19 is consistent with its ubiquitous expression pattern (Tian et al., 2003). It was shown that HDA19 is S-sulfenylated at Cys137 in plants treated with SA or flagellin 22 (flg22; Liu et al., 2015). It remains unclear how HDA19 undergoes redox modifications, and whether the modifications control its deacetylase activity and epigenetic function.

Under environmental stress, reactive oxygen and nitrogen species (ROS and RNS) are produced from various sources. Thiol (R-SH)-containing cysteine residues (Cys) are particularly prone to oxidation by ROS and RNS, which are often oxidized reversibly to sulfenic acid (R-SOH). Sulfenic groups can further form covalent bonds with nitric oxide (R-S-NO) called S-nitrosylation (Sevilla et al., 2015; Vaahtera et al., 2014). S-Nitrosylation affects protein function, including stability, biochemical activity, conformation change, subcellular localization and protein–protein interaction (Astier et al., 2011; Astier, Kulik, et al., 2012; Hess et al., 2005; Lamotte et al., 2015), and can mediate the physiological activity of NO that plays an important regulatory role in almost all aspects of development as well as response to stress in higher plants (Baxter et al., 2014; Couturier et al., 2013; Stamler et al., 2001; Wrzaczek et al., 2013). In the cell, S-nitrosylated glutathione (GSNO) is a more stable redox form of NO and is considered as a NO reservoir for protein S-nitrosylation (Feng et al., 2019). GSNO levels are controlled by the activity of S-nitrosogluthathione reductase (GSNOR) that catalyzes the NADH-dependent reduction of GSNO to oxidized GSH (GSSG; Jahnová et al., 2019; Lindermayr, 2018). The loss-of-function mutation of the unique gene in Arabidopsis leads to elevated levels of NO, increased protein S-nitrosylation, and pleiotropic effects on plant development and stress response (Feechan et al., 2005; Lee et al., 2008).

In this work, we show that HDA19 undergoes constitutive S-nitrosylation *in vivo*. We identified four S-nitrosylated Cys residues in the HDA19 protein purified from Arabidopsis cells by biotin-switch coupled with mass spectrometry. We found that SA and oxidative stress enhance HDA19 S-nitrosylation, binding to target loci, HDAC activity and gene repression function, in which the S-nitrosylated Cys137 plays an important role. In turn, HDA19 is required for maintaining cellular redox state and plant tolerance to the stress. Finally, our results indicate that HDA19 is not only a target of redox regulation but also controls cellular redox signaling for plant tolerance to stress.

RESULTS

HDA19 is S-nitrosylated and Cys137 is an important S-nitrosylated site

To study whether HDA19 undergoes S-nitrosylation, we transformed the *hda19* mutant with HDA19-HA under the control of a 2-kb promoter fragment of the gene but failed to get plants with sufficient expression of HDA19 and to complement the mutant phenotype. Therefore, we transformed the mutant with the 35S::HDA19-HA construct and obtained several complementation lines, among which lines C1 and C2 that produced a wild-type (WT) level of HDA19 transcripts and fully complemented the mutant phenotypes selected for further analysis (Figure S1a). We isolated HDA19-HA protein by immuno-purification from 10-day-old C1 and C2 seedlings, and processed Cys-S-nitrosylation TMT (Tandem Mass Tag) labeling reactions. The TMT biotin-switch analysis revealed a clear S-nitrosylation signal of HDA19-HA purified from the two complementation lines (Figures 1a and S1b). To study whether HDA19 S-nitrosylation is influenced by NO levels, transgenic plants expressing HDA19-HA were treated with the endogenous NO donor GSNO at 0.5 mM and the NO scavenger cPTIO (2-(4-carboxyphenyl)-4,4,5,5-tetramethylimidazoline-1-oxyl-3-oxide) at 0.25 mM for 45 min. Exogenously added GSNO enhanced HDA19-HA S-nitrosylation (Figures 1b and S1c), while cPTIO treatment abolished the S-nitrosylation signals (Figures 1c and S1d). To confirm the results, we transfected 35S::HDA19-HA into protoplasts prepared from the NO/GSNO accumulation- *gsnor* (At5g43940) mutant plants (Feechan et al., 2005), and detected a clear increase of HDA19-HA S-nitrosylation (Figures 1d and S1e), indicating that cellular NO accumulation stimulates HDA19 S-nitrosylation.

To detect the detail information of HDA19 S-nitrosylation, mass spectrometry (MS) analysis of the protein samples were performed. HDA19 Cys21, Cys137, Cys281 and Cys292 residues were found to be S-nitrosylated (Figure S2; Supplemental Dataset 1). HDA19 Cys281 and Cys292 are conserved in Arabidopsis and human HDAC proteins, while Cys137 is conserved in Arabidopsis HDA9 and human HDAC3. Cys21 is conserved only in human HDAC2 (Figure S2) and it does not locate in HDAC domain. Computational analysis of the putative HDA19 protein model revealed Cys137 and Cys21 were close to each other (Figure 1e), suggesting there might be mutual effect between these two sites. We also made Cys to Ala substitution of the four Cys residues and expressed the mutant versions (C21A/C137A/C281A/C292A-HA) in *hda19* protoplasts to test the mutation effect on HDA19 S-nitrosylation. TMT biotin-switch assays revealed that the C137A mutation had a stronger effect than the others (Figures 1f and S1f). To analyze the role of S-nitrosylation at Cys137, we transformed the *hda19* plants with the 35S::HDA19C137A-HA construct, and selected two lines (mC1 and mC2) that showed a C137A-HA protein level similar to that of

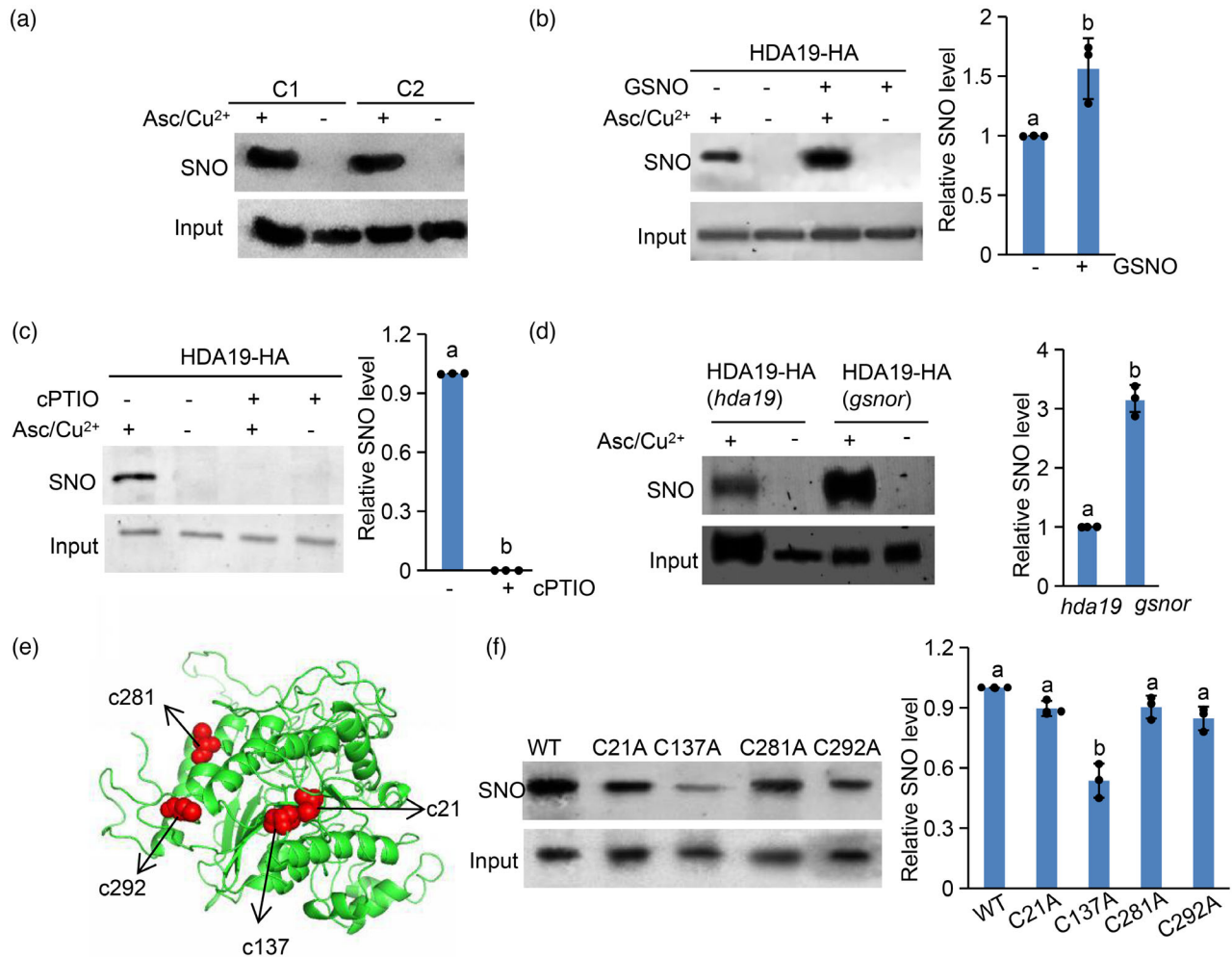


Figure 1. Identification of S-nitrosylated Cys residues in HDA19.

(a) Detection of HDA19 S-nitrosylation. HDA19-HA was immuno-purified with anti-HA from the HDA19-HA complementation plants (C1 and C2 lines), and was analyzed by TMT-labeling biotin-switch Western blots. The absence of ascorbate sodium (Asc) and 10 μ mol Cu²⁺ was used as technological negative control (-). Input protein levels were detected by anti-HA.

(b, c) S-Nitrosylation levels of HDA19-HA isolated from the complementation plants (C1 and C2 combined) treated with or without 0.5 mM GSNO (b) or 0.25 mM cPTIO (c) detected by TMT-labeling biotin-switch assays as in (a).

(d) S-Nitrosylation levels of HDA19-HA isolated from the *hda19* and *gsnor* mutant protoplasts transfected by the 35S::HDA19-HA vector.

(e) Computational modeling of the HDA19 protein. The four S-nitrosylated Cys residues (Cys21, Cys137, Cys281 and Cys292) of HDA19 revealed by mass spectrometry (MS) are indicated by red balls.

(f) Tests of Cys to Ala mutation effect at the four Cys residues on HDA19 S-nitrosylation by TMT-labeling biotin-switch assays. The proteins with point mutations were produced in and purified from transfected protoplasts of *hda19* plants. The other replicates of the immunoblots are shown in Figure S1. Western blot bands were quantified by ImageJ. Relative (optical density units relative to that of the inputs) average values from the three replicates are shown. The values of the wild-type (WT) protein (purified from line C2) are set at 1. Bars represent standard errors from three biological replicates (the value of each biological replicate was shown as black dots). Significant differences (represented by different letters) among multiple comparisons were tested by LSD (Fisher's least significant difference).

HDA19-HA in C1 and C2 plants (Figure S1g) and showed S-nitrosylation (Figure S1h) for further analysis. MS analysis of the C137A-HA protein purified from mC1 and mC2 plants detected only two S-nitrosylated Cys residues (Cys281 and Cys292; Figure S2; Supplemental Dataset 1), suggesting that the C137A mutation also affected S-nitrosylation at Cys21.

Because SA could induce HDA19 S-sulenylation at Cys137 (Liu et al., 2015), we also explored whether SA induces HDA19 S-nitrosylation. We treated the transgenic

plants with SA (0.5 mM) for 45 min, and found that SA enhanced S-nitrosylation of HDA19-HA and NO content (Figures 2a,b and S3a). However, SA hardly induced S-nitrosylation of C137A-HA, similarly the NO content was much lower in C137A-HA than HDA19-HA plants with or without SA, indicating that Cys137 is involved in SA-induced S-nitrosylation of the protein and also affected the intracellular NO level (Figures 2a,b and S3a). To study whether HDA19 S-nitrosylation is affected by oxidative stress, we treated leaves of the 19-day-old transgenic plants

with 3-amino-1,2,4-triazole (3-AT), a catalase inhibitor, at 2 mM for 36 h, and found that the treatment increased about 2.5-fold of the HDA19-HA S-nitrosylation levels and, to a lesser extent, that of C137A-HA (Figures 2c and S3b). 3-AT treatment also increased the NO level (Figure 2d). To further detect the effect of intracellular NO levels on HDA19 S-nitrosylation, different concentrations of NO scavenger cPTIO were added in 3-AT-treated plants. The results showed that cPTIO significantly abolished the S-nitrosylation signals of HDA19-HA and C137A-HA caused by 3-AT, and at the same concentration the cPTIO inhibitory effect was stronger in C137A-HA than in HDA19-HA (Figures 2e and S3c), confirming the higher NO contents in 3-AT-treated HDA19-HA than C137A-HA. To further confirm the oxidative stress effect on HDA19-HA S-nitrosylation, we transformed the *cat2* (At4g35090) mutant (which increased cellular oxidative state in seedlings; Li et al., 2014) with the *35S::HDA19-HA* vector and found that HDA19-HA S-nitrosylation was augmented about 2.4-fold in the *cat2* plants (Figures 2f and S3d). The NO content was also higher in the *cat2* plants than WT (Figure 2g).

Collectively, the results indicate that HDA19 is post-translationally modified by S-nitrosylation, and that SA and oxidative stress that enhance intracellular NO levels promote HDA19 S-nitrosylation. The C137A mutation reduced the levels of HDA19 S-nitrosylation under both normal and stressed conditions, and showed reduced intracellular NO levels.

Stress-induced HDA19 S-nitrosylation occurs mainly in the nucleus

To study HDA19 subcellular localization, we produced transgenic plants of *35S::HDA19-EGFP* and *35S::HDA19C137A-EGFP* in the *hda19* background (Figure S4a,b). Confocal microscopy revealed that HDA19-GFP and C137A-GFP proteins were localized in both nucleus and cytoplasm in the transgenic root cells and in transiently transfected protoplasts (Figures 3a and S4b). The 3-AT treatment enriched the nuclear localization of the proteins (Figure 3a). DAF-DA

analysis detected NO in the nucleus and the cytoplasm (Figure 3a), the levels of which were enhanced by 3-AT treatment (Figure 3a).

To further study subcellular localization of HDA19 S-nitrosylation, we isolated the total, cytoplasmic and nuclear protein fractions from the *HDA19-HA* and *C137A-HA* plants treated with or without 3-AT for biotin-switch analysis. The results revealed that under normal conditions HDA19-HA S-nitrosylation was detected in both nucleus and cytoplasm at a comparable level (Figures 3b and S4c), consistent with the protein distribution detected by microscopy observation (Figure 3a). After the 3-AT treatment, S-nitrosylated HDA19-HA was detected only in the nucleus. The 3-AT-induced nuclear S-nitrosylation levels of the protein were about four times higher than the untreated nuclear levels (Figure 3b), in line with the nuclear enrichment of NO and HDA19-EGFP under stress (Figure 3a). The C137A-HA S-nitrosylation was detected only in the nucleus under both normal and stressed conditions, probably due to the overall reduced S-nitrosylation levels of the mutant (Figure 2). The 3-AT treatment increased the C137A-HA S-nitrosylation levels only by about twofold (Figure 3b). The data indicate that the stress-induced HDA19 S-nitrosylation was enriched in the nucleus, and that besides C137 other Cys residues of the protein were also involved in the stress-induced S-nitrosylation.

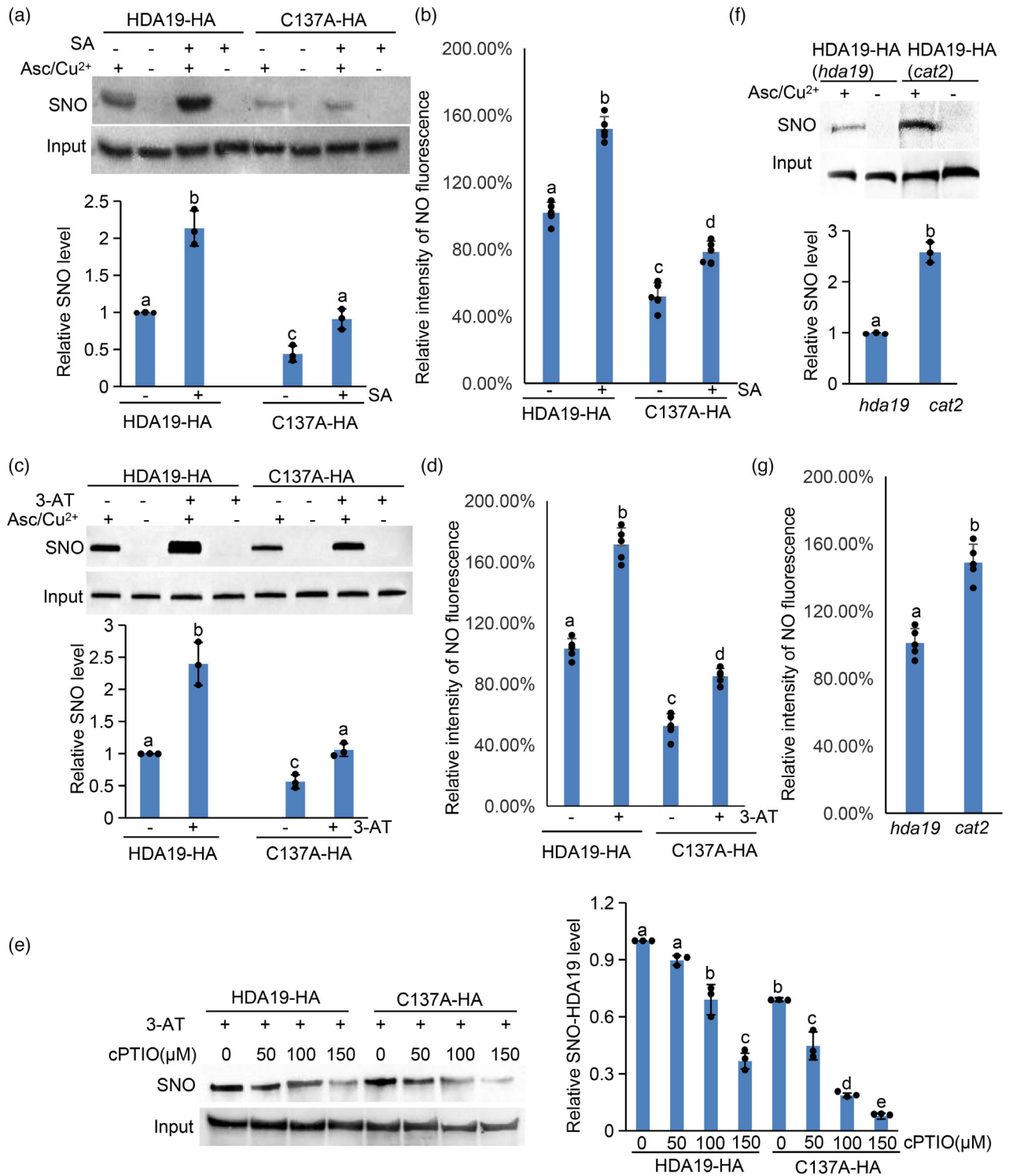
Cys137 is important for HDA19 function in controlling plant development and stress response

The *hda19* mutant plants display a number of developmental defects including meristem function, leaf, floral organ morphology, flowering time, plant height and trichome numbers (Ueda et al., 2018; Zhou et al., 2005; Figure S5a,b). We found that the mutant phenotypes were complemented by *HDA19-HA*, but only partially by *C137A-HA* (Figure S5a,b), indicating that Cys137 is required for the full function of HDA19 in plant development. To further evaluate the role of Cys137 in HDA19-regulated plant response to oxidative stress, we treated 19-day-old plants of the different genotypes with 3-AT.

Figure 2. HDA19 S-nitrosylation is enhanced by salicylic acid (SA) and oxidative stress.

- (a) S-Nitrosylation levels of HDA19-HA and C137A-HA proteins isolated from the complementation plants treated with or without 0.5 mM SA.
- (b) NO levels in the HDA19-HA and C137A-HA complementation plants treated with or without SA. The relative NO content was expressed with the fluorescence of the wild-type (WT; purified from line C2) set as 100%.
- (c) S-Nitrosylation levels of HDA19-HA and C137A-HA proteins isolated from the complementation plants treated with or without 2 mM 3-amino-1,2,4-triazole (3-AT).
- (d) NO levels in the *HDA19-HA* and *C137A-HA* plants treated with or without 3-AT as determined in (b).
- (e) S-Nitrosylation levels of HDA19-HA and C137A-HA proteins isolated from 2 mM 3-AT-treated plants after incubation with cPTIO at the different concentrations for 30 min.
- (f) HDA19-HA S-nitrosylation levels in the *cat2* mutant background.
- (g) NO level in the *hda19* and *cat2* mutant backgrounds.

The S-nitrosylation levels were analyzed by TMT-labeling biotin-switch Western blots, and the Western blot bands were quantified by ImageJ. The relative values (to the inputs) are averages of three separate experiments. (The other two replicates of the immunoblots are shown in Figure S3.) The NO content was detected using DAF-FM DA, and the relative NO content was expressed relative to the WT fluorescence (purified from line C2) set as 100%. Bars are means \pm SD from three independent experiments, and significant differences (represented by different letters) among multiple comparisons were tested by LSD (Fisher's least significant difference).



Based on the characteristic bleaching phenotype induced by 3-AT, we found that the sensitivity of the *hda19* mutant to 3-AT was the highest, while that of the WT and *HDA19-HA* plants was the lowest (Figures 4a and S5c). The sensitivity of

C137A-HA plants was at intermediate levels (Figures 4a and S5c), indicating that HDA19 is required for plant tolerance to the oxidative stress at least partly by maintaining cellular redox homeostasis under stress. DAB staining was

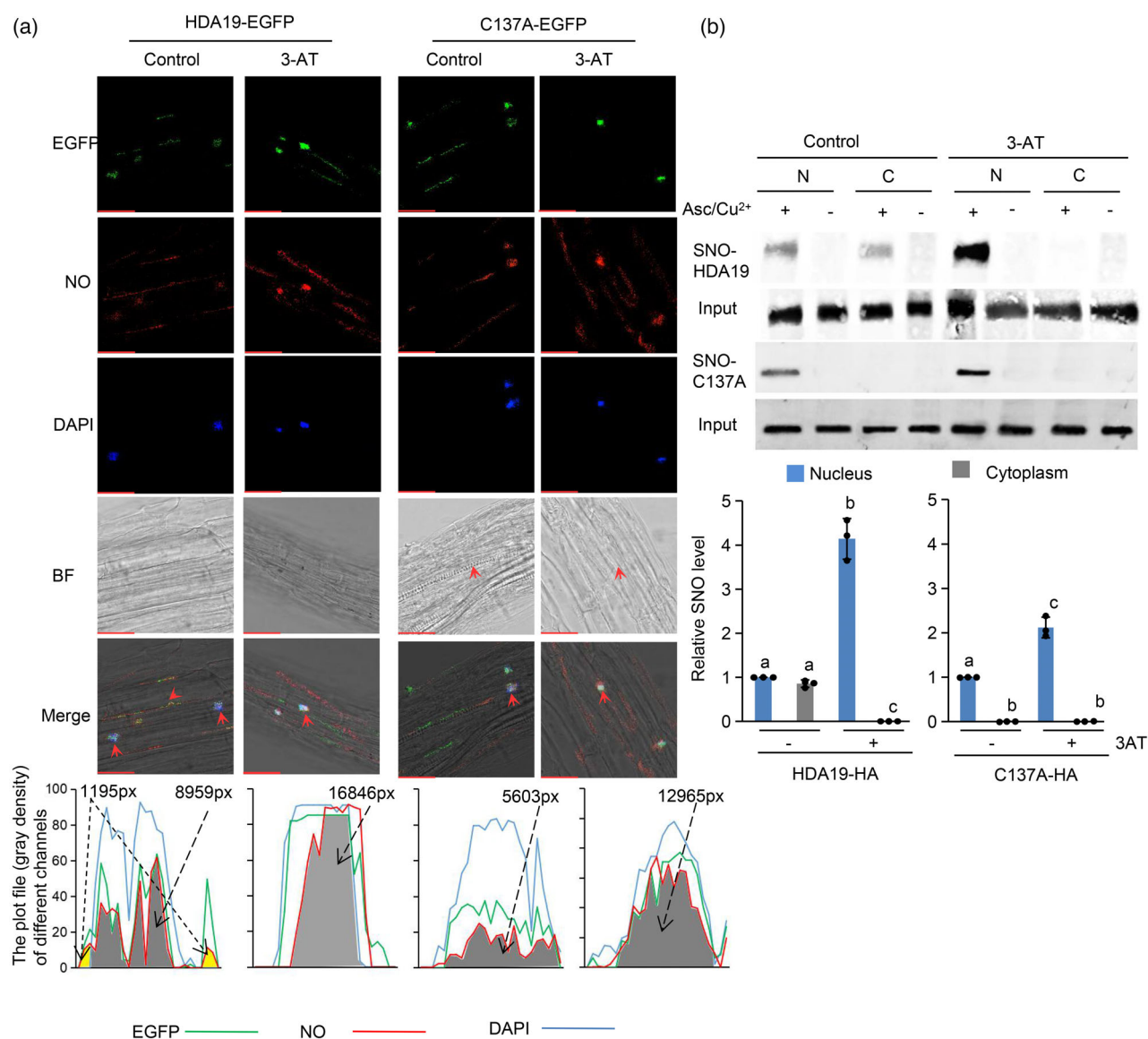


Figure 3. Stress-induced HDA19 S-nitrosylation takes place mainly in the nucleus.

(a) The subcellular localization of HDA19-EGFP, C137A-EGFP and NO detected by DAF-DA in HDA19-EGFP and C137A-EGFP complementation plants treated with or without 2 mM 3-amino-1,2,4-triazole (3-AT). The red arrows indicated the co-enrichment of NO and EGFP signals. The fluorescent plot files of different channels were calculated by the Leica SP8 software (Deerfield, IL, USA), the yellow areas represent S-nitrosylated HDA19 in cytoplasm (co-enrichment of EGFP and NO) and the gray areas represent S-nitrosylated HDA19 in the nucleus (co-enrichment of EGFP, DAPI and NO). Scale bars: 10 μ m.

(b) HDA19 S-nitrosylation levels in the cytoplasm and nucleus. Biotin-switch assays of S-nitrosylation levels of HDA19-HA and C137A-HA proteins immunoprecipitated from nuclear and cytoplasmic fractions extracted from plants treated with or without 2 mM 3-AT. The absence of ascorbate sodium (Asc) and 10 μ M Cu²⁺ are used as technological negative controls (-). Input protein levels were detected by anti-HA. The experiments were repeated independently three times, the other two replicates are shown in Figure S4(c). The Western blot bands were quantified by ImageJ. The relative values (optical density units relative to the optical density of the inputs) are averages of three separate experiments. The values of nuclear HDA19-HA or C137A-HA in the controls are set as 1. Bars represent standard errors from three biological replicates, and significant differences (represented by different letters) among multiple comparisons were tested by LSD (Fisher's least significant difference).

performed to detect the oxidative stress level in the plants caused by 3-AT treatment. Under normal conditions, there were no clear differences among the plant lines (Figure 4b). However, with 3-AT treatment the highest levels of staining were found in the *hda19* mutant, followed by *C137A-HA*, and the lowest levels were detected in *HDA19-HA* plants

(Figures 4b and S5d). Tests of chlorophyll contents of the different samples confirmed the sensibilities of the different plant lines to 3-AT (Figure S5e).

To explore the influence of HDA19 on overall cell redox state, we measured the contents of total and oxidized forms of glutathione, and determined the percentages of reduction

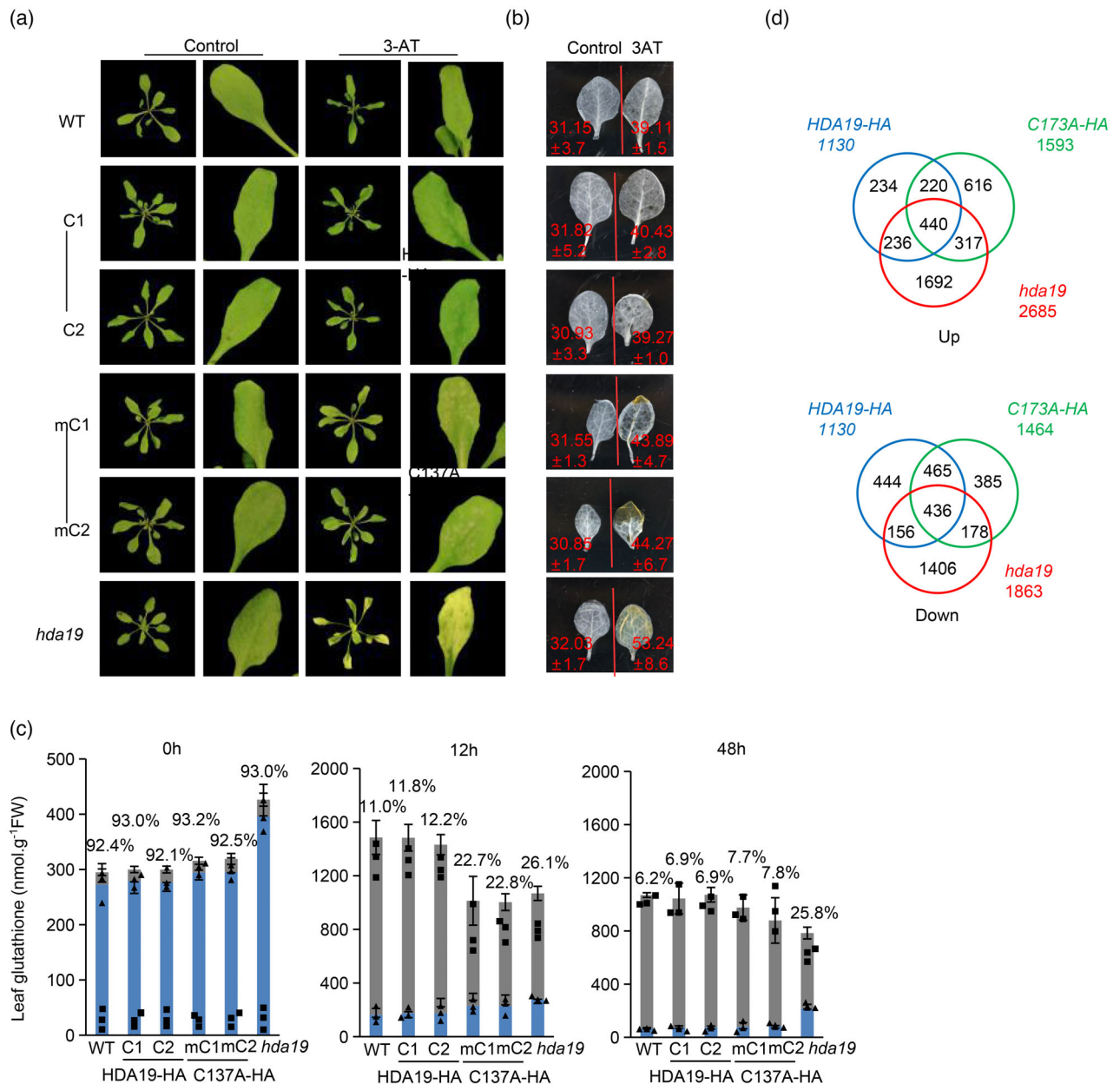


Figure 4. Cys137 is important for HDA19 function in oxidative stress tolerance and redox homeostasis.

(a, b) Leaf phenotypes and DAB (diaminobenzidine) staining of leaves isolated from 19-day-old wild-type (WT), complementation lines and the *hda19* mutant plants grown under normal conditions (control) or treated with 2 mM 3-amino-1,2,4-triazole (3-AT) for 36 h. Values represent quantification of DAB staining from three experiments measured using the luminosity function in Photoshop in arbitrary units with means \pm 2SE.

(c) Contents of total and oxidized glutathione in the plants of the above genotypes grown under normal (0 h) and oxidative stress conditions during 12 and 48 h. Blue and red blocks indicate, respectively, reduced and oxidized forms of glutathione. Percentages of the reduced form versus the total contents are indicated. Bars show means \pm SD from three independent experiments (the value of each experiment was shown as black rectangles or triangles).

(d) Venn diagrams of upregulated and downregulated genes in *HDA19*-HA (right), *C137A*-HA (middle) and *hda19* plants (left) treated by 3-AT.

of this key redox molecule in the different plants. Without 3-AT, there was about 92–93% of reduced glutathione in the different genotypes, although higher levels of total glutathione were observed in *hda19* plants (Figure 4c). After 12 h treatment, the total glutathione levels were markedly elevated in all genotypes, but the increase was less important in *hda19*

and *C137A*-HA plants compared with WT and *HDA19*-HA plants. In addition, the percentages of reduced glutathione in *hda19* (26.1%) and *C137A*-HA (22.7–22.8%) plants were about double of WT and *HDA19*-HA plants (11.0–12.2%). After 48 h treatment with 3-AT, the percentages of reduced glutathione in *hda19* (25.8%) were about triple of *C137A*-HA (7.7–7.8%),

HDA19-HA and WT plants (6.2–6.9%; Figure 4c). It is known that during oxidative stress, the glutathione pool is first oxidized by conversion from reduced to oxidized form, which retro-activates the biosynthetic enzyme, γ -glutamyl-cysteine synthetase, leading to an increase in total glutathione. The relatively less important increase in the total glutathione pool and the higher reduced glutathione levels in *hda19* and *C137A-HA* plants treated by 3-AT suggest that HDA19 is required for oxidative stress signaling to maintain cellular redox homeostasis and that Cys137 is important in the processes.

To investigate the role of Cys137 in HDA19-regulated oxidative stress-responsive gene expression, we performed RNA-seq analysis of the *hda19*, *HDA19-HA*, *C137A-HA* and WT (*Ws* ecotype) plants (Figure S6a,b). Consistent with previous analysis (Shen et al., 2019), the *hda19* mutation resulted in a large number of differentially expressed genes (DEGs; 3965 upregulated and 1776 downregulated) relative to WT (Figure S7a). By contrast, in the *HDA19-HA* complementation plants there were only 20 DEGs (> two-folds, $P < 0.01$) relative to the WT (Figure S7a), in accordance with the WT phenotype of the complementation lines (Figure S5). However, in *C137A-HA* complementation plants, we detected > 200 up- and > 200 downregulated (> twofold, $P < 0.01$) genes relative to *Ws* or *HDA19-HA* plants (Figure S7a). The *C137A-HA* DEGs are enriched for stress responses (Figure S7b). In addition, there were more DEGs in *hda19* relative to *Ws* or *HDA19-HA* than relative to *C137A-HA* plants (Figure S7a). Collectively, the analysis indicated the *C137A* mutation partially affected HDA19-dependent gene expression program. Because of the very little difference between *Ws* and *HDA19-HA* plants, we only treated *C137A-HA*, *hda19* and *HDA19-HA* plants with 3-AT for comparison. 3-AT treatment resulted in 2685 up- and 2176 downregulated genes in *hda19* plants, much more than those detected in *HDA19-HA* and *C137A-HA* plants (Figures 4d and S7c; Supplemental Dataset 2). In *C137A-HA* plants, the number of upregulated DEGs was higher than in *HDA19-HA* plants (Figures 4d and S7c). About 25% (676/2685) and 28% (77/2685) of the 3-AT-induced genes in *hda19* overlapped with those in *HDA19-HA* and *C137A-HA* plants (similar for 3-AT-repressed genes), respectively, while more than 58% of the *HDA19-HA* DEGs overlapped with those in *C137A-HA* (Figure 4d).

To further study the specific role of Cys137 for HDA19 function in gene expression, we performed gene set enrichment analysis (GSEA) of the DEGs. GSEA is a statistical method for determining whether a given gene set is significantly enriched in a list of marker genes ranked by their correlation with a phenotype of interest (Subramanian et al., 2005). The GSEA revealed that in 3-AT-treated *HDA19-HA* plants the oxidative stress response-related gene ontology (GO) terms (or gene sets) GO:0006979 (response to oxidative stress) and GO: 0000302 (response

to ROS; $|\text{NES}| > 1$) were enriched in the 3-AT repressed DEGs ($\text{NES} < 0$; Figure S8a, left). In 3-AT-treated *C137A-HA* lines, only GO: 0000302 (response to ROS) was enriched in the downregulated ($\text{NES} < 0$) DEGs (Figure S8b, left). In 3-AT-treated *hda19* plants, neither of the GO terms was detected in the DEGs. However, GO:0010167 (response to nitrate, $\text{NES} > 0$) was found to be enriched in 3-AT-induced genes in *hda19* mutant. The number of genes contributing to GO:0006979 term was the highest in *HDA19-HA*, followed by *C137A-HA* and the *hda19* mutant (Figure S8a–c, right panels). Conversely, the number of 3-AT-induced genes belonging to GO:0006979 was the highest in the *hda19* mutant, followed by *C137A-HA* and *HDA19-HA* (Figure S8a–c, right panels). The above analysis indicates that HDA19 has a function to repress subsets of oxidative stress-related genes under stress, and that the *C137A* mutation partially impairs this function.

S-Nitrosylation stimulates HDA19 deacetylase activity

Cys137 is located closely to the HDA19 catalytic residues (Figure S2). To study whether Cys137A mutation affects HDA19 function in histone deacetylation, we compared histone acetylation levels in WT, *HDA19-HA*, *C137A-HA* and *hda19* plants by Western blots using antibodies against H3K9ac and H3K14ac marks. The results indicated that the level of H3K14ac, but not H3K9ac, was clearly augmented in the *hda19* mutant compared with the WT plants (Figures 5a and S9a), indicating that HDA19 is mainly involved in the removal of H3K14ac. H3K14ac levels in *HDA19-HA* plants (C1, C2) were similar to WT, while those in the *C137A-HA* plants (mC1, mC2) were at the intermediate levels (Figures 5a and S9a), indicating that the *C137A* mutation partially affected the HDA19-mediated histone deacetylation in plant cells. Treatment of the plants with 3-AT enhanced while with DTT decreased the overall H3K14ac and H3K9ac levels in the different genotypes (Figures 5b and S9b), corroborating previous results that the redox stress inhibited the overall cellular HDAC activities (Mengel et al., 2017). Similarly, GSNO increased while cPTIO decreased the overall H3K14ac and H3K9ac levels in different genotypes. However, the effects of GSNO were the strongest in the *hda19* mutants (Figures 5c and S9c), implying that the HDA19 deacetylase activity in the WT background was stimulated by 3-AT. The data suggested that the inhibitory effect of GSNO on the overall HDAC activities was overwhelming relative to its stimulating effect on HDA19. To clarify the issue, we isolated the *HDA19-HA* and *C137A-HA* proteins by immunoprecipitation from the respective transgenic plants treated with or without 3-AT. The assays revealed a lower HDAC activity of *C137A-HA* than *HDA19-HA* (Figure 5d). To test whether S-nitrosylation had a direct effect on HDA19 deacetylase activity, we pre-incubated the proteins with the NO donor GSNO or the NO scavenger cPTIO before the

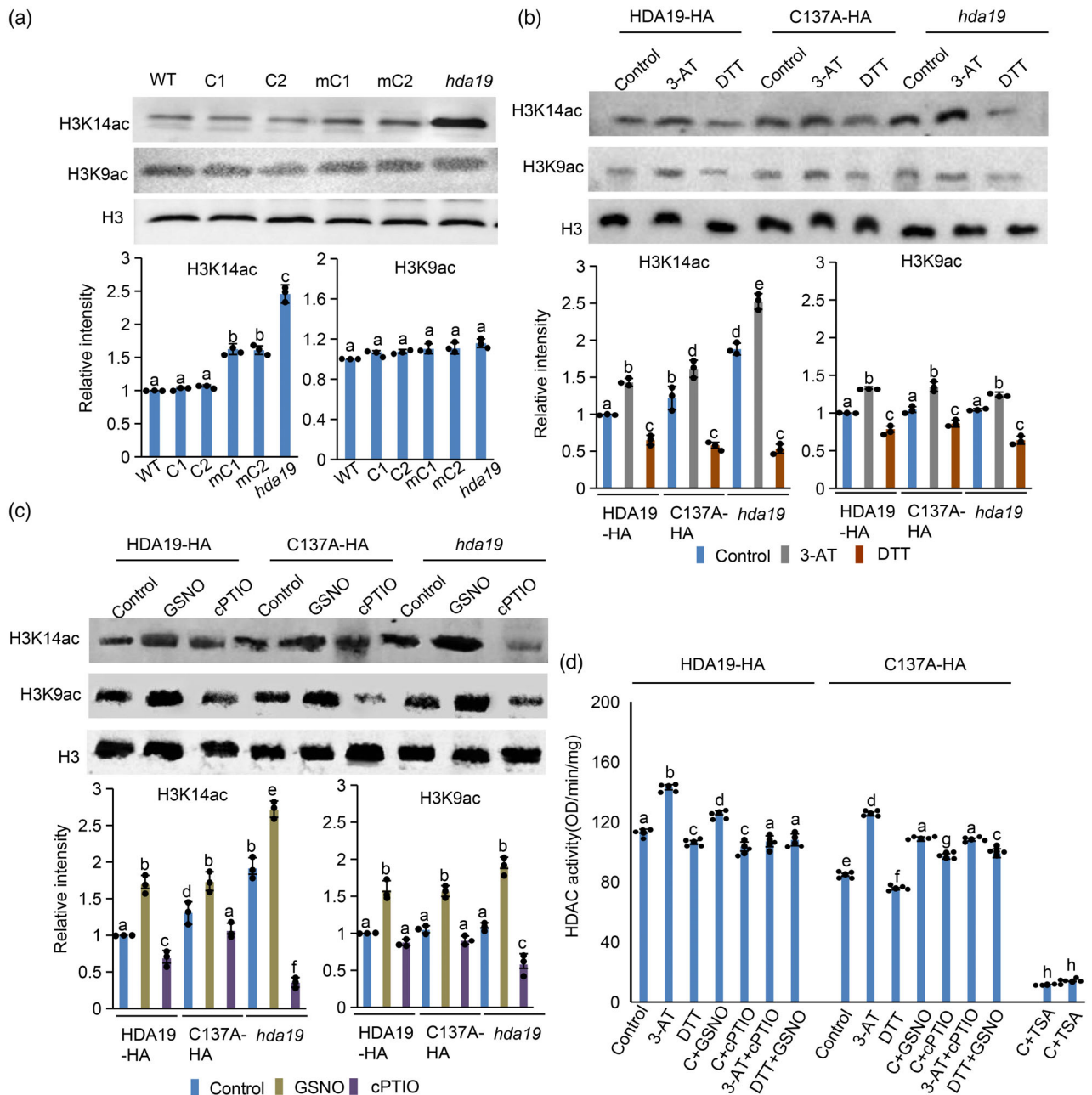


Figure 5. S-Nitrosylation enhances HDA19 histone deacetylase (HDAC) activity.

(a) Histone H3K14 and H3K9 acetylation levels in wild-type (WT), HDA19-HA (C1, C2) and C137A-HA (mC1, mC2) complementation, and *hda19* mutant plants grown under normal conditions. Histone acetylation levels were detected by immunoblots with anti-H3K14ac and anti-H3K9ac. Anti-H3 was used as control.

(b) Histone H3K14 and H3K9 acetylation levels in the plants treated with 3-amino-1,2,4-triazole (3-AT; 36 h) or DTT (36 h).

(c) Histone H3K14 and H3K9 acetylation levels in the plants treated with GSNO (45 min) or cPTIO (45 min). The Western blot bands were quantified by Image J. The relative values (optical density units relative to that of H3 histone) are averaged from three separate experiments (the other replicates are shown in Figure S8). The values of WT are set at 1. Bars represent standard errors from three biological replicates. Significant differences (represented by different letters) among multiple comparisons were tested by LSD.

(d) Tests of deacetylase activity of HDA19-HA and C137A-HA proteins (0.2 µg) purified by anti-HA immunoprecipitation from plants treated with or without 3-AT or DTT. The activities were also tested after incubation with 250 µM cPTIO for 30 min of the proteins from the 3-AT-treated (3AT + cPTIO) or with 250 µM GSNO for 30 min of proteins from DTT-treated (DTT + GSNO) and untreated control (C) (C + cPTIO or C + GSNO) plants. HDA19-HA and C137A-HA proteins purified from control plants were incubated with the HDAC inhibitor TSA at 100 µM as negative controls in the tests (C1 or C2 + TSA). The deacetylase activity was expressed as absorbance at 450 nm read on a microplate reader. Bars represent standard errors of five biological replicates (the value of each biological replicate was shown as black dots), and significant differences (represented by different letters) among multiple comparisons were tested by LSD.

activity tests. The presence of GSNO increased the deacetylase activity of HDA19-HA and C137A-HA isolated from untreated plants, and restored or partially restored the lower activities in DTT-treated plants. Conversely, cPTIO decreased the deacetylase activity of HDA19-HA isolated from 3-AT-treated and untreated plants (Figure 5d). cPTIO had no clear effect on the deacetylase activity of C137A-HA in the control plants but decreased the activity of the proteins isolated from 3-AT-treated plants, suggesting that S-nitrosylation stimulates the HDA19 deacetylase activity.

Next, we performed H3K14ac ChIP-seq analysis of *hda19* and the complementation plants (Figures S10 and S11; Table S1). Heat-maps of normalized ChIP-seq reads (RPKM) confirmed the slightly higher levels of H3K14ac in the *hda19* mutant than the transgenic plants, and higher levels in C137A-HA than HDA19-HA plants (Figures S12 and S13). More genes were found to be marked by H3K14ac in *hda19* (16065) and C137A-HA (14200) than in HDA19-HA (10081) plants (Figure S13b; Supplemental Dataset 3). Interestingly, 62.6% (5752/9188) genes that were marked by H3K14ac in *hda19* but not in HDA19-HA plants remained to be marked in C137A-HA plants (Figure S13b), indicating that C137A mutation impaired the HDA19-mediated deacetylation from a subset of genes. However, in 3-AT-treated plants, we observed an overall increase of H3K14ac in the three genotypes but still with the highest and lowest levels, respectively, observed in *hda19* and HDA19-HA plants (Figure S13a,b). The observations confirmed the Western blot results (Figure 5b), and supported the above observation that while inhibiting the overall HDAC activities, the oxidative stress imposed by 3-AT stimulated HDA19-mediated H3K14 deacetylation. These results also confirmed that the C137A mutation decreased the HDA19-mediated deacetylation. Pearson analysis between expression fold changes of the 317 genes that were induced by 3-AT commonly in *hda19* and C137A-HA but not in HDA19-HA plants, and fold changes of gene promoter H3K14ac levels caused by 3-AT in the respective plants revealed a moderate correlation ($R = 0.55$) in C137A-HA, a strong correlation ($R = 0.74$) in *hda19* mutant, and no correlation ($R = 0.11$) in HDA19-HA plants (Figure S14), indicating that the C137A mutation de-repressed these genes by affecting HDA19 deacetylase activity under the oxidative stress. GO enrichment analysis of H3K14ac peaks was also performed. The relative gene number (represented by gene ratio) was highest in *hda19* mutant, followed by C137A-HA, and the lowest in HDA19-HA with or without 3-AT treatment (Figure S13c), which was in agreement with the above observation (Figure S13a,b). There were two GO terms related to response to oxidative stress GO:0016614 (oxidoreductase activity acting on CH-OH group of donors) and GO:0008233 (peptidase activity) enriched in *hda19* mutant, one GO:0008233 (peptidase activity) enriched in C137A-HA and no related terms

enriched in HDA19-HA. Moreover, a higher relative gene number was induced by 3-AT in these two terms in the *hda19* and C137A-HA mutants than HDA19-HA plants (Figure S13c). Moreover, the numbers of GO terms induced by 3-AT was the lowest in HDA19-HA, followed by C137A-HA and the *hda19* mutant. The GO analysis of H3K14ac supported the results of Western blot (Figure 5b) and HDAC activity analysis (Figure 5d). To further study whether S-nitrosylation affects HDA19 binding to genomic loci, we performed anti-HA ChIP-seq analysis of the transgenic plants (Figures S10 and S11). We detected higher binding signals in HDA19-HA than C137A-HA plants (Figures S11 and S15a). The anti-HA ChIP-seq peaks corresponded to 2213 genes in HDA19-HA compared with 1402 genes in C137A-HA plants (Figure S15b; Supplemental Dataset 4). However, 60% (838/1402) of the C137A-HA binding genes overlapped with those bound by the WT version, suggesting that the C137A mutation reduced the HDA19 binding to a subset of the target genes, which is in agreement with the higher H3K14ac observed in C137A-HA than HDA19-HA plants. We found that 3-AT treatment stimulated the binding of both HDA19-HA and C137A-HA (with 2961 and 2450 genes bound by HDA19-HA and C137A-HA, respectively) and enabled the HDA19-binding to many new targets (Figure S15a). The GO analysis also revealed that 3-AT significantly increased the enriched genes both in HDA19-HA and C137A-HA. The 3-AT induced more enriched GO terms in HDA19-HA than in C137A-HA (Figure S15c). Moreover, the relative gene numbers of the GO terms directly related to deacetylation (GO:0019213, deacetylase activity; GO:0004407, HDAC activity; and GO:0033558, protein deacetylase activity) was the highest in 3-AT-treated-HDA19-HA, followed by 3-AT-treated-C137A-HA, the control-HDA19-HA, and finally the control-C137A-HA (Figure S15c). Interestingly, other GO terms, GO:0016810 [oxidoreductase activity acting on NAD(P)H] and GO:0050136 [NADH dehydrogenase (quinone) activity] were only enriched in 3-AT-treated HDA19-HA (Figure S15c). The results were consistent with the observations that 3-AT enhanced the localization and S-nitrosylation of HDA19 in the nucleus, and supported the above data that the oxidative stress stimulated the activity of HDA19 for genome-wide deacetylation.

Further analysis of the RNA-seq and ChIP-seq data identified 31 genes that showed repressed expression, reduced H3K14ac and increased HDA19-bindings in 3-AT-treated versus untreated HDA19-HA plants (Figure 6a; Supplemental Dataset 5). These genes were related to stress response (Figure 6b), and represented the downstream targets directly repressed by HDA19 under the stress. To validate the RNA-seq and the ChIP-seq data, we selected three of the target genes (*AtWRKY8*, *AtOZI1* and *AtCIPK4*) and one HDA19-independent oxidative stress responsive gene (*AtCAT2*) to test the 3-AT effects on their expression, H3K14ac and HDA19-binding levels by reverse

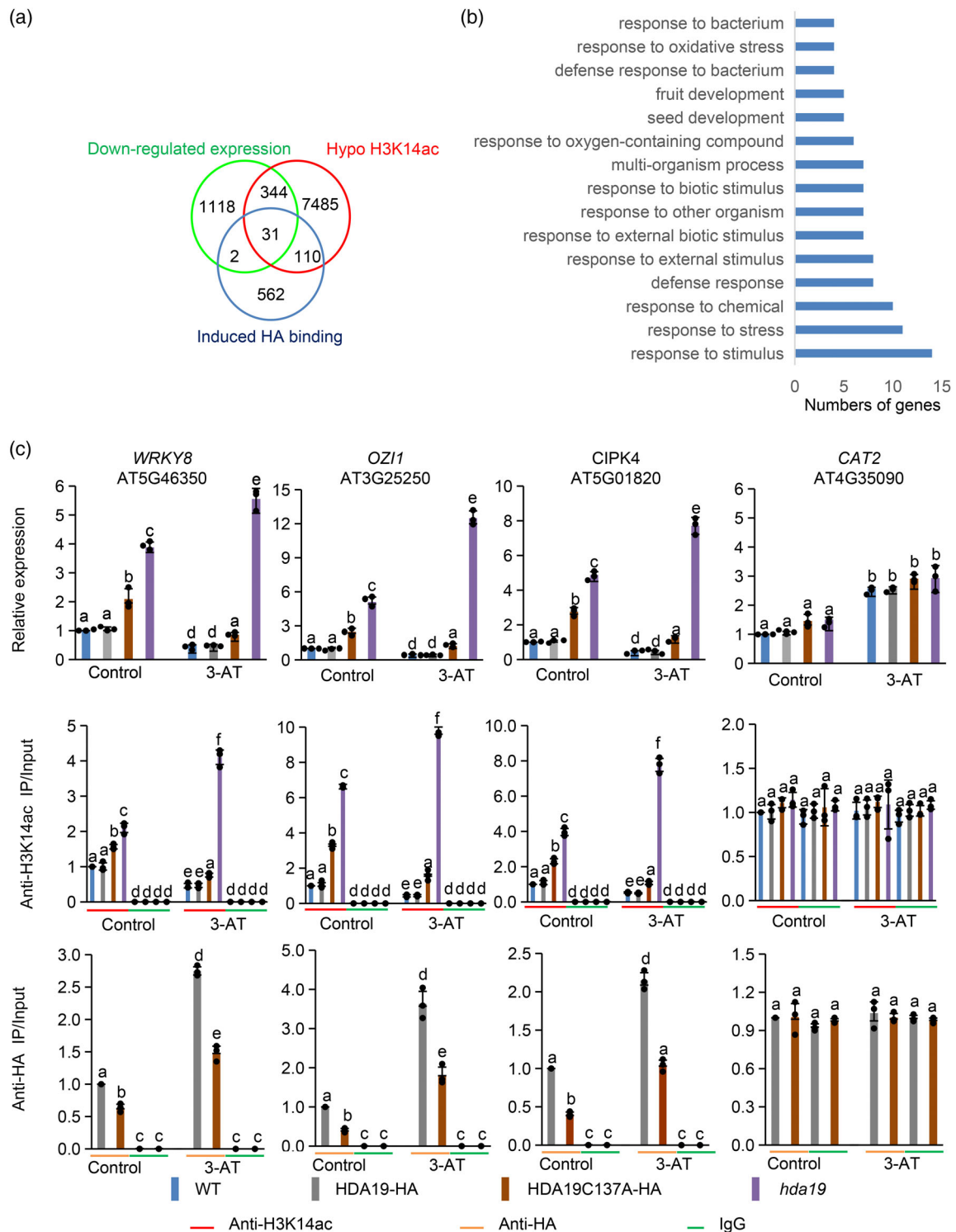


Figure 6. HDA19 directly represses several oxidative-stress responsive genes under both normal and stress conditions through histone H3K14 deacetylation. (a) Venn diagram of genes with downregulated expression, hypo H3K14ac and HDA19-HA binding in HDA19-HA plants induced by 3-amino-1,2,4-triazole (3-AT) in HDA19-HA. (b) Gene ontology (GO) analysis of the 31 overlapping genes in (a). (c) Reverse transcriptase-quantitative polymerase chain reaction (RT-qPCR) tests of transcript levels, chromatin polymerase chain reaction (ChIP-PCR) of H3K14ac levels and direct association of HDA19-HA and HDA19C137A-HA proteins of three of the 31 genes (*AtWRKY8*, *AtOZI1* and *AtCIPK4*) and an unrelated control gene (*AtCAT2*) in the different genotypes under normal or stressed (3-AT) conditions. IgG was used as control for ChIP-PCR assays. Bars represent means \pm SD from three biological replicates and multiple comparisons were conducted to compare significant differences among samples by LSD.

transcriptase-quantitative polymerase chain reaction (RT-qPCR) and chromatin immunoprecipitation-polymerase chain reaction (ChIP-PCR) in WT, *HDA19-HA*, *C137A-HA* and *hda19* plants (Figure 6). The transcript levels of *AtWRKY8*, *AtOZI1* and *AtCIPK4* were higher in *hda19* than in WT plants under both normal and stressed conditions. In *HDA19-HA* plants, the transcripts decreased back to WT levels, while in *C137A-HA* plants the transcript levels decreased only partially restored (Figure 6c, upper part). ChIP-qPCR analysis revealed that the H3K14ac levels correlated with the expression levels of the genes in both growth conditions (Figure 6c, middle part). Anti-HA ChIP-qPCR analysis indicated that these genes were bound by both *HDA19-HA* and *C137A-HA*, and that the *C137A-HA* binding appeared lower than *HDA19-HA* (Figure 6c, lower part). Treatment with 3-AT enhanced the binding of *HDA19-HA* and *C137A-HA* to these genes (Figure 6c, lower part). By contrast, although 3-AT treatment induced the expression of *AtCAT2*, no change was detected for H3K14ac or the *HDA19* binding in the 3-AT-treated plants (Figure 6c). Collectively, the analysis confirmed that *HDA19* directly represses a subset of oxidative stress-induced genes under both normal and stressed conditions through H3K14ac deacetylation, and that oxidative stress enhances the *HDA19-HA*-mediated repression by stimulating its HDAC activity and/or binding to the target loci.

DISCUSSION

HDA19 is an essential epigenetic regulator involved in a large panel of developmental processes and stress-responsive pathways in Arabidopsis. In this work we show that *HDA19* is post-translationally modified by S-nitrosylation and the modification is stimulated by oxidative stress. Because the cellular levels of NO were augmented under the oxidative stress (Figure 3a), we speculate that the increased NO levels stimulated *HDA19* S-nitrosylation, which in turn promoted the nuclear enrichment of the S-nitrosylated *HDA19* protein. Likely the stress-induced S-nitrosylation mostly occurred in the nucleus, although it is not excluded that S-nitrosylated *HDA19* promoted its import in the nucleus under stress. The observations that stress-stimulated *HDA19* S-nitrosylation enhances *HDA19* binding to genomic loci, HDAC activity and repression of stress-responsive genes indicate that *HDA19* chromatin regulatory function is modulated by S-nitrosylation. The data showing that Cys137 is a major site for both basal and stress-induced *HDA19* S-nitrosylation and that the *C137A* mutation affects plant development and stress response, suggest that Cys137 is important for *HDA19* function modulated by S-nitrosylation. This is supported by the observation that among the four Cys residues, the Cys137A mutation had a more important effect on *HDA19* S-nitrosylation and that the *C137A* mutation substantially decreased the 3-AT-induced *HDA19* S-nitrosylation in the nucleus (Figure 3b). In addition, the Cys137A mutation also

inhibits S-nitrosylation of Cys21 (Figure 1f), which are close in position in the structure model of *HDA19* (Figure 1e). Because C137 can be modified by S-sulfonylation (Liu et al., 2015), it is not excluded that the *C137A* mutation effect on the *HDA19* function may be also caused by reduced S-sulfonylation. However, this seems unlikely, as S-sulfonylation is extremely unstable (its identification actually requires prior alkylation to stabilize), which reacts rapidly to produce other forms such as S-nitrosylation. Alternatively, the *C137A* mutation may alter the *HDA19* protein structure, HDAC activity and target binding.

Our results are consistent with previous observations that *HDA19* plays a distinct role from that of class II RPD3 type HDACs (*HDA5/14/15/18*) in stress response (Choi et al., 2012; Ueda et al., 2018). This is supported by the requirement of *HDA19* for plant cellular redox homeostasis and tolerance to oxidative stress shown in this work. *HDA19* together with *HDA6* and *HDA9* belongs to a different RPD3 subgroup (closely related to human class 1 HDAC) from *HDA5/14/15/18* (related to human class 2 HDAC), which have distinct catalytic residues (Yruela Guerrero et al., 2021).

S-Nitrosylated proteins are involved in almost all developmental and stress-responsive processes (Albertos et al., 2015; Astier, Besson-Bard, et al., 2012; Astier, Kulik, et al., 2012; Berger et al., 2016; Cui et al., 2018; Iglesias et al., 2018; Lindermayr et al., 2010; Liu et al., 2017; Serrato et al., 2018). However, S-nitrosylation of most plant proteins was identified after NO donor treatment (Astier, Kulik, et al., 2012; Feng et al., 2019), and was based on recombinant proteins produced in prokaryotic cells, which displays some limitation (Sahdev et al., 2008; Willems et al., 2021). The present work identified four S-nitrosylated Cys residues in the *HDA19* protein produced in plant cells, a highest number of S-nitrosylated Cys residues ever characterized in plant proteins (Astier, Kulik, et al., 2012; Feng et al., 2019). This would suggest that either plant cell-produced proteins allow more exhaustive identification of S-nitrosylated sites or the number of S-nitrosylated Cys residues in *HDA19* is particularly high. It is suggested that S-nitrosylation of target proteins can be subtly regulated by biotic and abiotic stresses (Fares et al., 2011; Lee et al., 2008; Lindermayr et al., 2010; Liu et al., 2015; Tanou et al., 2009; Wang et al., 2009). The present data showing that *HDA19* S-nitrosylation is constitutive at a lower level but increased by stress indicate that S-nitrosylation is a robust post-translational modification of *HDA19*. S-Nitrosylation regulates protein activity, stability, localization and protein-protein interactions (Feng et al., 2019; Willems et al., 2021). For instance, S-nitrosylation facilitates NPR1 oligomerization in the cytoplasm to regulate immune response (Tada et al., 2008), represses AHP1 phosphorylation to control cytokinin response (Feng et al., 2013), enhances APX1 activity to increase resistance to oxidative stress (Yang et al., 2015), stimulates ASK1 binding to CUL1-TIR1 to take part in response to auxin (Iglesias et al., 2018),

induces autophagic degradation of GSNOR1 to adjust hypoxia response (Zhan et al., 2018), and increases activity of protein arginine methyltransferase5 (PRMT5) in stress tolerance (Hu et al., 2017). The observations that S-nitrosylation enhances the HDA19 genomic binding and deacetylase activity are reminiscent of the observation that S-nitrosylation at Cys125 of PRMT5 enhances its arginine methyltransferase activity (Hu et al., 2017). However, S-nitrosylation appeared to have distinct or opposing effects on mammalian HDAC proteins (Ago et al., 2008), suggesting that the effect of S-nitrosylation of HDACs may be dependent on the structural context of target proteins. Among conserved Cys residues, only the counterparts of HDA19 Cys 281 and 292 are acetylated in human HDACs (Ago et al., 2008). S-Nitrosylation of the N-terminal Cys21 and Cys137 that are not all conserved in plant or human HDACs (Figure 1b) may be specific to HDA19 and may affect HDA19 activity differently from other HDACs, especially Cys137 that is located in the HDAC activity motif (Figure S2).

Collectively, our results indicate that oxidative stress such as exogenously applied 3-AT enhanced the cellular NO levels that stimulated S-nitrosylation of HDA19. HDA19 S-nitrosylation promoted its nuclear enrichment and enhanced its HDAC activity to repress expression of subsets of genes to improve plant tolerance to the stress (Figures 4 and 7). We speculate that HDA19-mediated HDAC may be required to repress genes whose expression is unfavorable for stress tolerance, or to attenuate the acute induction of stress-responsive genes whose excessive or continuous expression might be harmful for the cell. Alternatively, HDA19 may repress the expression of transcription factors or metabolic or redox genes that play negative roles in stress tolerance.

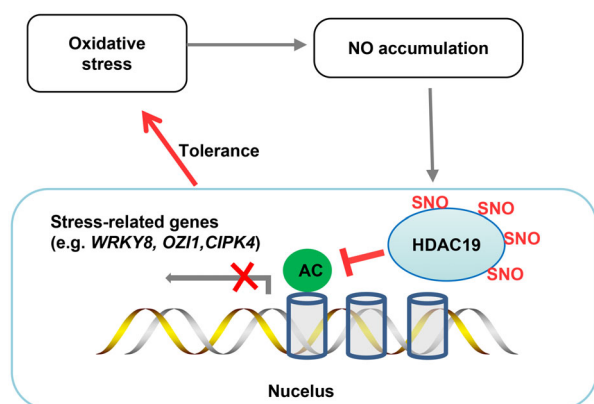


Figure 7. Proposed model of HDA19 response to oxidative stress. Oxidative stress [such as 3-amino-1,2,4-triazole (3-AT) treatment] leads to NO accumulation in cells, which enhances S-nitrosylation of HDA19. Stress-induced S-nitrosylation stimulates HDA19 nuclear enrichment and histone deacetylase (HDAC) activity to remove H3K14ac and to repress the expression of a set of genes of which an excessive or continuous expression is unfavorable for plant tolerance. Red: functions of S-nitrosylated HDA19.

EXPERIMENTAL PROCEDURES

Plant materials, production of transgenic plants, treatments and phenotype analysis

The Arabidopsis ecotype Wassilewskija (Ws) was used as WT in this study. The *hda19* (At4g38130, *hda19* or *athd1*, in *Ws* background), *gsnor* (At5g43940, *gsnor-1*, in *Columbia-0*, *Col.0* background) and *cat* (At4g35090, *cat2-1*, in *Col.0* background) T-DNA mutants were previously reported (Feechan et al., 2005; Li et al., 2014; Shen et al., 2019). To produce complete complementation plants, the full-length cDNA of AtHDA19 was amplified and cloned into p1301-35S-HA and p1301-35S-EGFP vector (F: AAAGTCGACGAT ACTGGCGGCAATTCGCTG; R: TTGCGGCCGCGCTTATGTTT TAGG AGGAAACGC). These vectors were transformed by Agrobacterium-mediated infection of *hda19* mutant plants to obtain over-expression (complementation HDA19-HA lines). Cysteine 137 of HDA19 cDNA was mutated to alanine (C137A) using the QuikChange Site-Directed Mutagenesis Kit (Agilent Technologies, Beijing, China; cat#210518) and the 35S::C137A-HA construct was transformed into *hda19* plants to obtain point the C137A-HA lines. After surface-sterilization in 30% bleach, Arabidopsis seeds were kept at 4°C for 48 h before sowing. The seeds were grown *in vitro* on half-strength Murashige Skoog with 0.5% sucrose media (pH 5.7, 1.2% agar) in a growth chamber (20°C) under white light (120 $\mu\text{mol m}^{-2} \text{sec}^{-1}$ photons) in 16 h light/day photoperiods for 10 days, and transplanted into soil or sampled for further analysis. For trichome density analysis, trichomes were counted and calculated from the largest leaf of four plants randomly selected from each genotype.

For SA treatment, 10-day-old seedlings grown in MS medium were treated with 0.5 mM SA for 3 h. For GSNO and cPTIO treatment, 10-day-old seedlings grown in 1/2 Murashige Skoog medium were treated with 0.5 mM GSNO or 0.25 mM cPTIO for 45 min. For redox treatments, 19-day-old plants (a stage that plants became tolerant to the treatment) grown in soil were treated by spraying the leaves with 2 mM 3-AT or 10 mM DTT. After 36 h, plants were photographed and harvested for mRNA, proteins or chromatin extractions or measurements of glutathione contents and chlorophyll content or DAB staining. The total and oxidized glutathione levels were measured according to previously reported methods (Zheng et al., 2020). The DAB staining was conducted as previously described (Torres et al., 2002). For chlorophyll content determination, about 100 mg leaves were excised into 2–3 cm length, and then were immersed in the extract solution (45% ethanol + 45% acetone + 10% water) at room temperature until the leaves were bleached. The absorbance of the extracts was read at 647 and 665 nm. The total chlorophyll content was then calculated (Inskeep & Bloom, 1985).

Determination of endogenous NO content

The endogenous NO level was analyzed by using an NO-sensitive dye, DAF-FM DA (Chandok et al., 2003). For DAF-FM DA imaging, Arabidopsis samples were collected 8 h after dawn, incubated in a solution containing 0.1 mM CaCl_2 , 10 mM KCl, 10 mM MES-Tris, pH 5.6 for 2 h, stained with 20 mM DAF-FM DA (Abcam, Shanghai, China; ab145388) for 1 h, and rinsed three times with distilled water. The treated leaves were analyzed using confocal (Leica SP8). The excitation was provided at 560 nm, and the emission images at 595 nm were obtained with a constant acquisition time. To avoid fluorescent color cascades as much as possible, GFP fluorescence was excited at 480 nm and detected at 507 nm. The plot files of different channels were calculated by the Leica SP8 software. The relative content of NO was determined as described previously (Besson-Bard et al., 2009). To follow NO production in

leaf discs, 7-mm-diameter leaf discs excised from *Arabidopsis* plants grown on soil were infiltrated for 30 min with 10 mM DAF-FM DA dissolved in the solution described above. Then, leaf discs were incubated for 1 h in the dark, rinsed three times with distilled water, and transferred in the dark into a 96-well plate (one disc per well) containing 200 µl of distilled water. NO production was measured by using a fluorometer (Molecular Device Company, San Jose, CA, USA; Spectra Max M2) with 485 nm excitation and 510 nm emission filters. Twelve leaf discs were used for each treatment. Fluorescence was expressed as relative fluorescence units (RFU). All experiments were repeated at least three times.

In vivo S-nitrosylation detection using TMT switch assay

All the proteins used for S-nitrosylation detection including total proteins, nuclear proteins and cytoplasmic proteins were extracted from 15 g seedling tissues (for Western blot) or 10×10^8 protoplasts (for LC-MS and Western blot) of 35S::HDA19-HA and 35S::C21A/C137A/C281A/C292A-HA plants using the extraction kit (BestBio, Beijing, China; cat#BB319905, cat#BB319906) according to the manufacturer's instructions. To improve the efficiency of protoplast transformation, 5 µl of carrier DNA ($10 \mu\text{g } \mu\text{l}^{-1}$) was added to 50 µl of transformation system. About 300 µg isolated native proteins were immunoprecipitated with 6 µl commercial Anti-HA Magnetic Beads (ThermoFisher Scientific, Waltham, MA, USA; cat#88838) at 4°C overnight to purify HDA19-HA or C137A-HA protein followed the non-denaturing purification protocol from manufacturer's instructions with purification buffer (BestBio; cat#BB3204). To maintain native structure of HDA19-HA/C137A-HA for S-nitrosylation analysis, all the above commercial buffers were free of reductive agent. After being concentrated, proteins were used for S-nitrosylation detection by an improved biotin-switch technique (ThermoFisher Scientific; cat#90105). The brief pipeline of S-nitrosylation detection biotin-switch assay was as follows: (i) blocking of native -SHs by MMTS (methyl methanethiosulfonate); (ii) reduction of Cys-SNOs by ascorbate with the help of Cu^{2+} ; and (iii) labeling of the newly generated Cys-SHs from Cys-SNOs with sufficient iodoTMT.

For LC-MS analysis, the TMT-labeled S-nitrosylated proteins were enriched by vacuum freeze-drying before Western blot detection using anti-TMT (ThermoFisher Scientific; cat#90075) or LC-MS analysis. An aliquot of the (5 µl) proteins was used for Western blot to confirm the S-nitrosylation signal, the rest was purified (from Coomassie-stained gels) for LC-MS analysis. After digestion at 37°C for 4 h using trypsin and desalination using C18 spin tips, Cys-TMT proteins were resuspended in TBS and enriched using anti-TMT antibody resin (ThermoFisher Scientific; cat#90076) overnight with end-over-end shaking at 4°C. After collection of the unbound peptides, the resin was washed four times with 4 M Urea/TBS, four times with 0.05% CHAPS, four times with TBS, and four times with water. Finally, labeling peptides were eluted four times with 50% acetonitrile, 0.4% TFA and then dried under vacuum before LC-MS/MS analysis.

Western blot

For HDA19 subcellular localization analysis, nuclear and cytoplasmic proteins of the same amounts of seedlings as for total protein extraction were extracted using Plant Nuclear and Cytoplasmic Protein Extraction Kit (BestBio; cat#BB-3152-1). Protein extracts were separated by sodium dodecyl sulfate-polyacrylamide gel electrophoresis (SDS-PAGE) or with non-reducing native gels (Criterion™ XT Tris-Acetate Precast Gels; Cat# 3450129 and Native Sample Buffer for Protein Gels; Cat# 1610738) and analyzed by Western blots using Anti-HA (Abcam; ab9110, 1:5000) to detect the

HDA19-HA. As controls, Anti-actin (cytoplasmic fraction, Abcam; ab197345, 1:5000) and Anti-H3 (nuclear fraction, Abcam; ab1791, 1:5000) were used.

For histone acetylation analysis, histone proteins were extracted from 1.5 g plant tissues as using Plant Histone extraction kit (BestBio; cat#BB31171). The following histone antibodies were used: H3K14ac (Millipore, Darmstadt, Germany; 2 686 926, 1:2000), H3K9ac (Millipore; 2686925, 1:2000), H3 (Abcam; ab1791, 1:5000). Because the different anti-histone H3 acetylation antibodies detect the same protein/band, we had to use individual gel/membrane for each immunoblot. For the sample loading controls, we first performed anti-H3 Western blots and used the signals to calibrate sample loading for the experiments with the antibodies of acetylated H3.

All Western blots were developed using the ECL Super signal system with 50–100 µg protein sample. Western blot bands were measured and quantified by the ImageJ software. The ratio of the integrated band density of the target protein to that of the reference protein or input was used to normalize band intensities. Each test was performed with three independent experiments, and the multiple comparisons using LSD (Fisher's least significant difference) method were conducted to compare significant differences among samples.

Tests of HDAC activity assay

The HDAC activity was determined by following the previous protocol (Zheng et al., 2020). The HDAC inhibitor TSA (100 nM) was used as control. The absorbance was read on a microplate reader within 2–10 min at 450 nm. Total nuclear proteins (about 5 µg) extracted from 35S::HDA19-HA, 35S::C137A-HA and *hda19* seedlings were used to test total HDAC activity. HDA19 proteins (0.2 µg) immunopurified from 35S::HDA19-HA and 35S::C137A-HA plants grown under normal and stressed conditions were used to test HDAC activity. To determine the direct impact of S-nitrosylation on HDAC activity of HDA19, purified proteins from normal and 3-AT-treated samples were incubated with 250 µM cPTIO for 30 min, and proteins from normal and DTT-treated samples were incubated with 250 µM GSNO for 30 min before the activity tests.

Protein structural modeling

Homology modeling of three-dimensional structure HDA19 based on their sequence similarity to five proteins of known structure downloaded from PDB database (<http://www.rcsb.org/>). Homology modeling was performed with MODELER (<https://salilab.org/modeller/>). This model with the lowest energy and highest score was selected for further docking analysis. ZDOCK (<http://zdock.umassmed.edu/>) was used for primary docking, and the top1 model produced by ZDOCK was optimized by PyROSETTA (<http://www.pyrosetta.org/>) according to the software's protein-protein interaction protocol. Structural figures were prepared using PyMOL (<https://pymol.org/2/>).

RNA-seq and RT-qPCR experiments

Total RNA was extracted from seedlings using Trizol reagents and for RNA-seq analysis. For RNA-seq library construction, 2 µg of total RNA was used for mRNA purification and cDNA synthesis. Then the mRNA was enriched by using oligo (dT) magnetic beads. Mixed with the fragmentation buffer, the mRNA was broken into short fragments (about 200 bp). The first strand of cDNA was synthesized by using random hexamer primer. Buffer, dNTPs, RNase H and DNA polymerase I were added to synthesize the second strand. The double-strand cDNA was purified with magnetic

beads. End reparation and 3'-end single nucleotide A (adenine) addition was performed. Finally, sequencing adaptors were ligated to the fragments. The fragments were enriched by PCR amplification. The library products were sequenced with the Illumina HiSeq 2000 platform, and the library construction and sequencing were completed at Novogene (Tianjin, China). Two independent biological replicates were produced.

For quantitative real-time PCR (qRT-PCR) assays, the cDNA was synthesized from 1 µg of total RNA using the First Strand cDNA Synthesis Kit (Transgene Biotech, Beijing, China). Transcript levels were normalized against the average of the reference genes: the tubulin and actin genes (AT5G62690 and AT3G18780). The Ct values and the real-time PCR efficiencies were obtained using LinRegPCR (12.X) software, and then the normalized relative quantities and standard errors for each sample were obtained by pBaseplus software. The relative fold differences for genes expression in different samples were calculated on the base of the normalized relative quantities obtained above, with the normalized relative quantity of WT (control) as 1. There were two independent biological replicates, and each biological replicate had three technical repetitions, and reaction mixtures with double distilled water as templates were used as negative controls to evaluate the specificity of each real-time PCR.

ChIP-seq experiments

Chromatin fragments were isolated from seedlings of WT and mutant or transgenic plants, and immunoprecipitated with the following antibodies: H3K14ac (Millipore; 2686926) and HA (Abcam; ab9110) according to the previous method (Cui et al., 2021). IgG (Abcam; ab171870) was used as negative control.

The ChIP-seq products were sequenced by Novogene. The DNA was combined with End Repair Mix and incubated at 20°C for 30 min, purified the end-repaired DNA with QIAquick PCR Purification Kit (Qiagen, Beijing, China), added A-Tailing Mix and incubated at 37°C for 30 min. We combined the purified Adenylate 3' Ends DNA, Adapter and Ligation Mix and incubated the ligation reaction at 20°C for 15 min. Several rounds of PCR amplification with PCR Primer Cocktail and PCR Master Mix were performed to enrich the Adapter-ligated DNA fragments. Then the PCR products were selected (about 100–500 bp, including adaptor sequence) by running a 2% agarose gel to recover the fragments. We purified the gel with QIAquick Gel Extraction kit (Qiagen). The final libraries were sequenced with the Illumina HiSeq 2000 platform. The amounts of immunoprecipitated chromatin fragments relative to input chromatin were also determined by qPCR analysis using primer pairs specific to target genes, and calculated according to the 2^{-ΔΔCT} method. Each test was performed with three biological replicates.

Bioinformatic analysis of high-throughput sequence reads

For bioinformatics analysis of the RNA-seq and ChIP-seq data, clean reads were obtained by removing reads containing adapter, reads containing poly-N and low-quality reads from raw data, and were aligned to the Arabidopsis genome (The Arabidopsis Information Resource, <http://www.arabidopsis.org/index.jsp>) using FastQC software. The software subread, featureCounts and Deseq were subsequently used for RNA-seq data analysis, and genes with an FDR ≤ 0.01 and fold change ≥ 2 were designated as DEGs. The software Bowtie2, MACS, IGV, ChIPseeker were used for ChIP-seq data analysis. The input group was used as a positive control and IgG as a negative control for ChIP. IP signal/input signal were calculated to perform gene-body enrichment analysis. GO analysis were performed with clusterProfile and R software.

For Pearson correlation analysis, the upregulated peaks of H3K14ac were found by MACS2 and normalized by Deseq with fold change > 1 and *q* < 0.05. The normalized fold change of upregulation peaks of H3K14ac and log2 fold change value of DEGs were then used for further analysis.

LC-MS/MS and data processing

For protein complex analysis, immunoprecipitation proteins were freeze-dried at -70°C for enrichment. After being fully trypsinized, the proteins were analyzed on Thermo Fisher LTQ Orbitrap ETD MS. Briefly, samples were loaded onto an HPLC chromatography system named Thermo Fisher Easy-nLC 1000 equipped with a C18 column (1.8 mm, 0.15 × 1,00 mm). Solvent A contained 0.1% formic acid and solvent B contained 100% acetonitrile. The elution gradient was from 4% to 18% in 182 min, 18% to 90% in 13 min solvent B at a flow rate of 300 nL min⁻¹. MS analyses were carried out at the AIMS Scientific (Shanghai, China) in the positive-ion mode with an automated data-dependent MS/MS analysis with full scans (350–1600 *m/z*) acquired using FTMS at a mass resolution of 30 000 and the 10 most intense precursor ions were selected for MS/MS. The MS/MS was acquired using higher-energy collision dissociation at 35% collision energy at a mass resolution of 15 000. Raw MS files were analyzed by Proteome Discoverer 1.4 with TAIR data (uniprot-Arabidopsis thaliana.fasta). The related parameters used for raw MS files analyzed were as follows: EnFLAGme Name was Trypsin (full); Max.Missed Cleavage Sites were 2; Static Modification was Carbamidomethyl (C); Dynamic Modification were Oxidation (M), Deamidated (N, Q), Acetyl(K); Precursor Mass Tolerance was 20 ppm; Fragment Mass Tolerance was 0.05 D; Validation based on *q*-value. Each sample had two biological replicates to ensure the accuracy.

AUTHOR CONTRIBUTIONS

YZ, ZL and XC performed most of the experiments; AD, El-B, CB, ZY, XL, LP and GC-I participated in the experiments; D-XZ, El-B, J-PR, GN and HV designed the experiments and analyzed the data; D-XZ and El-B supervised the work; D-XZ and ZY wrote the paper.

ACKNOWLEDGEMENTS

This study was supported by National Natural Science Foundation of China (NSFC31701100), French Agence National de la Recherche (ANR-196CE12-0027-01), State Scholarship Fund of China Scholarship Council (CSC 201708420299), Team foundation of Jiangnan University (03100074), High Level Incubation Program of Jiangnan University (3015/06210049). The authors thank Dr T. Lei for her contribution to this study.

CONFLICT OF INTEREST

The authors declare that they have no conflict of interest.

SUPPORTING INFORMATION

Additional Supporting Information may be found in the online version of this article.

Figure S1. Production of HDA19-HA and HDA19C137A-HA transgenic plants in *hda19* mutant background. (a) Characterization of HDA19-HA complementation transgenic plants. 35S promoter was used to drive HDA19 cDNA translationally linked to 6 × HA. The vectors were transformed into the *hda19* plants. Five positive lines

were tested by qRT-PCR for HDA19 expression in comparison with the WT and *hda19* mutant plants. C1 and C2 lines that show a HDA19 expression similar to the WT were selected. (b–e) The other two replicates of Figure 1(a–d). (f) The other replicates of Figure 1(f). Vectors for production of HDA19-HA C21A, C137A, C281A and C292A mutant proteins are shown. (g) Protein levels in two independent complementation lines of HDA19-HA and HDA19C137A-HA transgenes (in *hda19* mutant background) were detected by Western blot using anti-HA. (h) Detection of S-nitrosylation of HDA19C137A-HA protein immuno-purified with anti-HA from the complementation plants (mC1 and mC2 lines) by biotin-switch assays.

Figure S2. Sequence alignment of Arabidopsis HDA19, HDA6, HDA9 and HDA15 together with human HDAC2 and HDAC3. The four S-nitrosylated Cys residues (Cys21, Cys137, Cys281 and Cys292) of HDA19 revealed by mass spectrometry are indicated by red arrows. The HDA19 putative catalytic residues His148, His149 and Try311 are indicated by blue arrows, and the putative Zn²⁺-binding residues are indicated by purple arrows. Conserved Cys residues and their flanking sequences are highlighted by yellow. The red box represents the histone deacetylase domain superfamily (IPR003084).

Figure S3. Time course of SA and 3-AT treatment to determine the optimal timing for sampling and the other two replicates of Figure 2.

Figure S4. Characterization of HDA19-EGFP and C137A-EGFP plants and other two replicates of Figure 3. (a) Characterization of HDA19-EGFP and C137A-EGFP complementation transgenic plants. The 35S promoter was used to drive HDA19 cDNA translationally linked to EGFP. The vectors were transformed into the *hda19* plants. Four positive lines were tested by Western blot for HDA19-EGFP expression in comparison with the WT and *hda19* mutant plants. 19E1 and C137AE2 were selected in this study. (b) The subcellular localization of HDA19-EGFP and C137A-EGFP in Arabidopsis protoplasts. (c) The other two replicates of Figure 3(b).

Figure S5. Phenotype of HDA19-HA and C137A-HA transgenic plants in the *hda19* mutant background. (a) Rosette phenotypes of WT, 35S::HDA19-HA (C1, C2), 35S::C137A-HA (mC1, mC2) and the *hda19* mutant plants. The trichome densities were counted and calculated for one leaf of four 19-day-old plants randomly selected from each genotype ($n = 4$). Bars represent means \pm SD from the five (plants) replicates (the value of each replicate was shown as black dots), and multiple comparisons were conducted to compare significant differences among samples. (b) Flower, silique and mature plant phenotypes of the complementation lines (C1, mC1) compared with WT and *hda19* mutant plants. (c, d) The other two repeated experiments of Figure 4(a,b), respectively. (e) Chlorophyll contents of different samples. Bars represent means \pm SD from the five (plants) replicates (the value of each replicate was shown as black dots), and multiple comparisons were conducted to compare significant differences among samples.

Figure S6. RNA-seq analysis of WT, *hda19* mutant and the complementation plants. (a) RNA-seq reads of HDA19-HA, C137A-HA transgenic and *hda19* mutant seedling grown at 20°C for 19 days, then treated 3-AT or not treated for 36 h before RNA extraction. (b) Pair-wise scatter plots of RNA-seq reads between three biological repeats. Each point represents one gene locus. RPKM, reads per kilobase per million reads. Correlation coefficient R^2 is indicated.

Figure S7. Differential gene expression in HDA19-HA, C137A-HA and *hda19* plants. (a) Volcano map of differentially expressed genes in between WT, *hda19*, HDA19-HA and C137A-HA plants as indicated. (b) GESA of DEGs of C137A-HA versus Ws. The top 10

increased and decreased significant gene sets were listed according to their NES (normalized enrichment score). The color of each bar represents the P -value of the gene set. The significance of each gene set was classified by a threshold of $P < 0.05$. (c) Volcano map of differentially expressed genes (DEGs, red dots) between control and 3-AT treatment of HDA19-HA (right), C137A-HA (middle) and *hda19* plants (left). (d) Venn diagrams of upregulated and downregulated DEGs in (c).

Figure S8. Differential gene expression in HDA19-HA, C137A-HA and *hda19* plants. Left panels: GESA analysis of DEGs of 3-AT treatment versus control in HDA19-HA (a), C137A-HA (b) and *hda19* (c) plants. The top 10 increased and decreased significant gene sets were listed according to their NES. The color of each bar represents the P -value of the gene set. The significance of each gene set was classified by a threshold of $P < 0.05$. Right panels: the GESA analysis of the 3-AT caused DEGs belonging to the GO term of oxidative stress response (GO:0006979) in HDA19-HA (a), C137A-HA (b) and *hda19* (c) plants. The positive/negative values of Y-axis (ranked list metric) represent up/downregulated DEGs induced by 3-AT, and the X-axis (position in ranked list of genes) represented the list of DEGs belonging to GO:0006979. The red dot vertical lines indicate the enrichment score (ES) values of DEGs in GO:0006979.

Figure S9. The other two replicates of data shown in Figure 6(a–c).

Figure S10. Correlation analysis of anti-H3K14ac and anti-HA ChIP-seq data. (a–c) Analysis of anti-H3K14ac and anti-HA ChIP-seq reads of HDA19-HA, C137A-HA plants and *hda19* mutant plants. Seedlings were grown at 20°C for 19 days, then treated with or without 3-AT for 36 h. IgG was used as control for the ChIP experiments. Pairwise scatter plots of ChIP-seq reads between two biological repeats are shown. Each point represents one gene locus. RPKM, reads per kilobase per million reads. Correlation coefficient R^2 indicated.

Figure S11. IDR analysis of anti-H3K14ac and anti-HA ChIP-seq reads. Pairwise scatter plots of ChIP-seq IDR log10 score between two biological repeats are shown. Red meant ≥ 0.05 IDR. The ratio of peaks passing IDR cutoff of 0.05 indicated. (a) HDA19-HA; (b) C137A-HA; (c) *hda19*.

Figure S12. ChIP-seq analysis of H3K14ac and HDA19-HA and C137A-HA binding profiles in *hda19* and/or HDA19-HA and C137A-HA plants. Left: metaplots of anti-H3K14ac and anti-HA ChIP-seq reads near the transcriptional start sites (TSS). The Y-axis is log2 (IP/Input signal). Right: IGV of the anti-H3K14ac peaks at AT3G46487 and AT5G07700 loci (upper part) and the anti-HA peaks at AT5G08130 and AT5G08139 loci (scales are indicated).

Figure S13. S-Nitrosylation induced by oxidative stress enhances total H3K14ac level. (a) Heatmaps of the H3K14ac ChIP-seq reads (normalized RPKM) in the *hda19* mutant and the complementation (by HDA19-HA or C137-HA) plants treated with or without 3-AT. TES, transcription end site; TSS, transcription start site. (b) Venn diagram of gene promoter H3K14ac peaks in plants of the *hda19* mutant and the complementation plants treated with or without 3-AT. (c) GO enrichment analysis of H3K14ac ChIP peaks among different samples under control (C) or 3-AT treatment (T) using peaks annotation analysis according to ChIP-seq data. The top 12 enrichment gene sets were listed by P -values. The area of dots represents the gene ratio, and the color of dots represents the P -value of the gene set. The significance of each gene set was classified by a threshold of $P < 0.05$ for H3K14ac. The red letters represented the crucial GO terms of response to oxidative stress.

Figure S14. Pearson correlation analysis of expression and H3K14ac levels of the 317 upregulated genes only observed in C137A-HA and *hda19* mutant. The Y-axis stands for log2-fold

change of gene expression levels, and the X-axis stands for normalized upregulated fold change of H3K14ac peaks in their promoter region caused by 3-AT. The dots whose value < 1 were not drawn in the plot.

Figure S15. S-Nitrosylation induced by oxidative stress enhances HDA19 binding activity. (a) Heatmaps of the genome-wide enrichment of anti-HA ChIP-seq reads (normalized RPKM) in the *HDA19-HA* and *C137A-HA* plants treated with or without 3-AT. (b) Overlapping between HDA19-HA- and C137A-HA binding genes under the control and 3-AT treatment are shown by the Venn diagrams on the left. Overlapping of HDA19-HA- or C137A-HA-binding genes between untreated and 3-AT-treated conditions are shown by the Venn diagrams on the right. (c) GO enrichment analysis of HA ChIP peaks among different samples under control (C) or 3-AT treatment (T) using peaks annotation analysis according to ChIP-seq data. The top 12 enrichment gene sets were listed by *P*-values. The area of dots represents the gene ratio, and the color of dots represents the *P*-value of the gene set. The significance of each gene set was classified by a threshold of $P < 0.05$ for HA. The red letters represented the crucial GO terms related to deacetylation.

Table S1 ChIP-seq reads and correlation coefficients between the replicates

Supplemental Dataset 1. MS graphs of SNO peptides of HDA19-HA and C137A-HA.

Supplemental Dataset 2. Lists of DEG in HDA19-HA compared with WT under normal conditions, and HDA19-HA, C137A-HA and *hda19* plants treated with and without 3-AT.

Supplemental Dataset 3. Anti-H3K14ac ChIP-seq annotation gene list.

Supplemental Dataset 4. Anti-HA ChIP-seq annotation gene list.

Supplemental Dataset 5. The information of 31 overlapping genes in Figure 6(a).

Supplemental Dataset 6. The full Western blot images in this study.

Supplemental Dataset 7. The primers used in this study.

OPEN RESEARCH BADGES



This article has earned an Open Materials badge for making publicly available the components of the research methodology needed to reproduce the reported procedure and analysis. All materials are available at TAIR (<https://conf.phoenixbioinformatics.org/pages/viewpage.action?pageId=8160428>).

DATA AVAILABILITY STATEMENT

The RNA-seq and the ChIP-seq data are deposited to National Genomics Data Center databases (PRJCA005948/PRJCA005893). The MS files are uploaded to the iProX databases (IPX0003322000/PXD027558).

REFERENCES

Ago, T., Liu, T., Zhai, P., Chen, W., Li, H., Molkentin, J.D. et al. (2008) A redox-dependent pathway for regulating class II HDACs and cardiac hypertrophy. *Cell*, **133**, 978–993.

Albertos, P., Romero-Puertas, M.C., Tatematsu, K., Mateos, I., Sánchez-Vicente, I., Nambara, E. et al. (2015) S-nitrosylation triggers ABI5 degradation to promote seed germination and seedling growth. *Nature Communications*, **6**, 1–10.

Alinsug, M.V., Yu, C.-W. & Wu, K. (2009) Phylogenetic analysis, subcellular localization, and expression patterns of RPD3/HDA1 family histone deacetylases in plants. *BMC Plant Biology*, **9**, 37.

Astier, J., Besson-Bard, A., Lamotte, O., Bertoldo, J., Bourque, S., Terenzi, H. et al. (2012) Nitric oxide inhibits the ATPase activity of the chaperone-like AAA+ ATPase CDC48, a target for S-nitrosylation in cryptogam signalling in tobacco cells. *Biochemical Journal*, **447**, 249–260.

Astier, J., Kulik, A., Koen, E., Besson-Bard, A., Bourque, S., Jeandroz, S. et al. (2012) Protein S-nitrosylation: what's going on in plants? *Free Radical Biology and Medicine*, **53**, 1101–1110.

Astier, J., Rasul, S., Koen, E., Manzoor, H., Besson-Bard, A., Lamotte, O. et al. (2011) S-nitrosylation: an emerging post-translational protein modification in plants. *Plant Science*, **181**, 527–533.

Baxter, A., Mittler, R. & Suzuki, N. (2014) ROS as key players in plant stress signalling. *Journal of Experimental Botany*, **65**, 1229–1240.

Benhamed, M., Bertrand, C., Servet, C. & Zhou, D.-X. (2006) Arabidopsis GCN5, HD1, and TAF1/HAF2 interact to regulate histone acetylation required for light-responsive gene expression. *The Plant Cell*, **18**, 2893–2903.

Berger, H., De Mia, M., Morisse, S., Marchand, C.H., Lemaire, S.D., Wobbe, L. et al. (2016) A light switch based on protein S-nitrosylation fine-tunes photosynthetic light harvesting in *Chlamydomonas*. *Plant Physiology*, **171**, 821–832.

Besson-Bard, A., Gravot, A., Richaud, P., Auroy, P., Duc, C., Gaymard, F. et al. (2009) Nitric oxide contributes to cadmium toxicity in Arabidopsis by promoting cadmium accumulation in roots and by up-regulating genes related to iron uptake. *Plant Physiology*, **149**, 1302–1315.

Chandok, M.R., Ytterberg, A.J., van Wijk, K.J. & Klessig, D.F. (2003) The pathogen-inducible nitric oxide synthase (iNOS) in plants is a variant of the P protein of the glycine decarboxylase complex. *Cell*, **113**, 469–482.

Choi, S.M., Song, H.R., Han, S.K., Han, M., Kim, C.Y., Park, J. et al. (2012) HDA19 is required for the repression of salicylic acid biosynthesis and salicylic acid-mediated defense responses in Arabidopsis. *The Plant Journal*, **71**, 135–146.

Couturier, J., Chibani, K., Jacquot, J.-P. & Rouhier, N. (2013) Cysteine-based redox regulation and signaling in plants. *Frontiers in Plant Science*, **4**, 105.

Cui, B., Pan, Q., Clarke, D., Villarreal, M.O., Umbreen, S., Yuan, B., et al. (2018) S-nitrosylation of the zinc finger protein SRG1 regulates plant immunity. *Nature Communications*, **9**, 1–12.

Cui, X., Zheng, Y., Lu, Y., Issakidis-Bourguet, E. & Zhou, D.-X. (2021) Metabolic control of histone demethylase activity involved in plant response to high temperature. *Plant Physiology*, **185**(4), 1813–1828. <https://doi.org/10.1093/plphys/kiab020>

Fares, A., Rossignol, M. & Peltier, J.-B. (2011) Proteomics investigation of endogenous S-nitrosylation in Arabidopsis. *Biochemical and Biophysical Research Communications*, **416**, 331–336.

Feechan, A., Kwon, E., Yun, B.-W., Wang, Y., Pallas, J.A. & Loake, G.J. (2005) A central role for S-nitrosothiols in plant disease resistance. *Proceedings of the National Academy of Sciences of the United States of America*, **102**, 8054–8059.

Feng, J., Chen, L. & Zuo, J. (2019) Protein S-nitrosylation in plants: current progresses and challenges. *Journal of Integrative Plant Biology*, **61**, 1206–1223.

Feng, J., Wang, C., Chen, Q., Chen, H., Ren, B., Li, X. et al. (2013) S-nitrosylation of phosphotransfer proteins represses cytokinin signaling. *Nature Communications*, **4**, 1–9.

Gao, M.-J., Li, X., Huang, J., Gropp, G.M., Gjetvåg, B., Lindsay, D.L. et al. (2015) SCARECROW-LIKE15 interacts with HISTONE DEACETYLASE19 and is essential for repressing the seed maturation programme. *Nature Communications*, **6**, 7243.

Gonzalez, D., Bowen, A.J., Carroll, T.S. & Conlan, R.S. (2007) The transcription corepressor LEUNIG interacts with the histone deacetylase HDA19 and mediator components MED14 (SWP) and CDK8 (HEN3) to repress transcription. *Molecular and Cellular Biology*, **27**, 5306–5315.

Gorham, S.R., Weiner, A.I., Yamadi, M. & Krogan, N.T. (2018) HISTONE DEACETYLASE 19 and the flowering time gene FD maintain reproductive meristem identity in an age-dependent manner. *Journal of Experimental Botany*, **69**, 4757–4771.

Hess, D.T., Matsumoto, A., Kim, S.-O., Marshall, H.E. & Stamler, J.S. (2005) Protein S-nitrosylation: purview and parameters. *Nature Reviews Molecular Cell Biology*, **6**, 150–166.

Hu, J., Yang, H., Mu, J., Lu, T., Peng, J., Deng, X. et al. (2017) Nitric oxide regulates protein methylation during stress responses in plants. *Molecular Cell*, **67**(702–710), e704.

- Iglesias, M.J., Terrile, M.C., Correa-Aragunde, N., Colman, S.L., Izquierdo-Álvarez, A., Fiol, D.F. et al. (2018) Regulation of SCFTIR1/AFBs E3 ligase assembly by S-nitrosylation of Arabidopsis SKP1-like1 impacts on auxin signaling. *Redox Biology*, **18**, 200–210.
- Inskip, W.P. & Bloom, P.R. (1985) Extinction coefficients of chlorophyll a and b in N, N-dimethylformamide and 80% acetone. *Plant Physiology*, **77**, 483–485.
- Jahnová, J., Luhová, L. & Petrivalský, M. (2019) S-nitrosoglutathione reductase—the master regulator of protein S-nitrosation in plant NO signaling. *Plants*, **8**, 48.
- Jang, I.-C., Chung, P.J., Hemmes, H., Jung, C. & Chua, N.-H. (2011) Rapid and reversible light-mediated chromatin modifications of Arabidopsis *Phytochrome a* locus. *The Plant Cell*, **23**, 459–470.
- Kim, K.-C., Lai, Z., Fan, B. & Chen, Z. (2008) Arabidopsis WRKY38 and WRKY62 transcription factors interact with histone deacetylase 19 in basal defense. *The Plant Cell*, **20**, 2357–2371.
- Krogan, N.T., Hogan, K. & Long, J.A. (2012) APETALA2 negatively regulates multiple floral organ identity genes in Arabidopsis by recruiting the co-repressor TOPLESS and the histone deacetylase HDA19. *Development*, **139**, 4180–4190.
- Lamotte, O., Bertoldo, J.B., Besson-Bard, A., Rosnoblet, C., Aimé, S., Hichami, S. et al. (2015) Protein S-nitrosylation: specificity and identification strategies in plants. *Frontiers in Chemistry*, **2**, 114.
- Lee, U., Wie, C., Fernandez, B.O., Feelsch, M. & Vierling, E. (2008) Modulation of nitrosative stress by S-nitrosoglutathione reductase is critical for thermotolerance and plant growth in Arabidopsis. *The Plant Cell*, **20**, 786–802.
- Li, S., Mhamdi, A., Trotta, A., Kangasjärvi, S. & Noctor, G. (2014) The protein phosphatase subunit PP 2A-B' γ is required to suppress day length-dependent pathogenesis responses triggered by intracellular oxidative stress. *New Phytologist*, **202**, 145–160.
- Lindermayr, C. (2018) Crosstalk between reactive oxygen species and nitric oxide in plants: key role of S-nitrosoglutathione reductase. *Free Radical Biology and Medicine*, **122**, 110–115.
- Lindermayr, C., Sell, S., Müller, B., Leister, D. & Durner, J. (2010) Redox regulation of the NPR1-TGA1 system of Arabidopsis thaliana by nitric oxide. *The Plant Cell*, **22**, 2894–2907.
- Liu, J.-Z., Duan, J., Ni, M., Liu, Z., Qiu, W.-L., Whitham, S.A. et al. (2017) S-nitrosylation inhibits the kinase activity of tomato phosphoinositide-dependent kinase 1 (PDK1). *Journal of Biological Chemistry*, **292**, 19743–19751.
- Liu, P., Zhang, H., Yu, B., Xiong, L. & Xia, Y. (2015) Proteomic identification of early salicylate- and flg22-responsive redox-sensitive proteins in Arabidopsis. *Scientific Reports*, **5**, 8625.
- Long, J.A., Ohno, C., Smith, Z.R. & Meyerowitz, E.M. (2006) TOPLESS regulates apical embryonic fate in Arabidopsis. *Science*, **312**, 1520–1523.
- Mehdi, S., Derkacheva, M., Ramström, M., Kraleman, L., Bergquist, J. & Hennig, L. (2016) The WD40 domain protein MS1 functions in a histone deacetylase complex to fine-tune abscisic acid signaling. *The Plant Cell*, **28**, 42–54.
- Mengel, A., Ageeva, A., Georgii, E., Bernhardt, J., Wu, K., Durner, J. et al. (2017) Nitric oxide modulates histone acetylation at stress genes by inhibition of histone deacetylases. *Plant Physiology*, **173**, 1434–1452.
- Mikkelsen, T.S., Ku, M., Jaffe, D.B., Issac, B., Lieberman, E., Giannoukos, G. et al. (2007) Genome-wide maps of chromatin state in pluripotent and lineage-committed cells. *Nature*, **448**, 553–560.
- Pandey, R., Müller, A., Napoli, C.A., Selinger, D.A., Pikaard, C.S., Richards, E.J. et al. (2002) Analysis of histone acetyltransferase and histone deacetylase families of Arabidopsis thaliana suggests functional diversification of chromatin modification among multicellular eukaryotes. *Nucleic Acids Research*, **30**, 5036–5055.
- Perrella, G., Lopez-Vernaza, M.A., Carr, C., Sani, E., Gossel, V., Verduyn, C. et al. (2013) Histone deacetylase complex1 expression level titrates plant growth and abscisic acid sensitivity in Arabidopsis. *The Plant Cell*, **25**, 3491–3505.
- Pi, L., Aichinger, E., van der Graaff, E., Llavata-Peris, C.I., Weijers, D., Hennig, L. et al. (2015) Organizer-derived WOX5 signal maintains root columella stem cells through chromatin-mediated repression of CDF4 expression. *Developmental Cell*, **33**, 576–588.
- Ryu, H., Cho, H., Bae, W. & Hwang, I. (2014) Control of early seedling development by BES1/TPL/HDA19-mediated epigenetic regulation of ABI3. *Nature Communications*, **5**, 4138.
- Sahdev, S., Khattar, S.K. & Saini, K.S. (2008) Production of active eukaryotic proteins through bacterial expression systems: a review of the existing biotechnology strategies. *Molecular and Cellular Biochemistry*, **307**, 249–264.
- Serrato, A.J., Romero-Puertas, M.C., Lázaro-Payo, A. & Sahravy, M. (2018) Regulation by S-nitrosylation of the Calvin-Benson cycle fructose-1, 6-bisphosphatase in *Pisum sativum*. *Redox Biology*, **14**, 409–416.
- Sevilla, F., Camejo, D., Ortiz-Espin, A., Calderón, A., Lázaro, J.J. & Jiménez, A. (2015) The thioredoxin/peroxiredoxin/sulfiredoxin system: current overview on its redox function in plants and regulation by reactive oxygen and nitrogen species. *Journal of Experimental Botany*, **66**, 2945–2955.
- Shen, Y., Lei, T., Cui, X., Liu, X., Zhou, S., Zheng, Y. et al. (2019) Arabidopsis histone deacetylase HDA 15 directly represses plant response to elevated ambient temperature. *The Plant Journal*, **100**, 991–1006.
- Song, C.-P., Agarwal, M., Ohta, M., Guo, Y., Halfter, U., Wang, P. et al. (2005) Role of an Arabidopsis AP2/EREBP-type transcriptional repressor in abscisic acid and drought stress responses. *The Plant Cell*, **17**, 2384–2396.
- Stamler, J.S., Lamas, S. & Fang, F.C. (2001) Nitrosylation: the prototypic redox-based signaling mechanism. *Cell*, **106**, 675–683.
- Subramanian, A., Tamayo, P., Mootha, V.K., Mukherjee, S., Ebert, B.L., Gillette, M.A. et al. (2005) Gene set enrichment analysis: a knowledge-based approach for interpreting genome-wide expression profiles. *Proceedings of the National Academy of Sciences of the United States of America*, **102**, 15545–15550.
- Tada, Y., Spoel, S.H., Pajerowska-Mukhtar, K., Mou, Z., Song, J., Wang, C. et al. (2008) Plant immunity requires conformational charges of NPR1 via S-nitrosylation and thioredoxins. *Science*, **321**, 952–956.
- Tanaka, M., Kikuchi, A. & Kamada, H. (2008) The Arabidopsis histone deacetylases HDA6 and HDA19 contribute to the repression of embryonic properties after germination. *Plant Physiology*, **146**, 149–161.
- Tanou, G., Job, C., Rajjou, L., Arc, E., Belghazi, M., Diamantidis, G. et al. (2009) Proteomics reveals the overlapping roles of hydrogen peroxide and nitric oxide in the acclimation of citrus plants to salinity. *The Plant Journal*, **60**, 795–804.
- Tian, L., Wang, J., Fong, M.P., Chen, M., Cao, H., Gelvin, S.B. et al. (2003) Genetic control of developmental changes induced by disruption of Arabidopsis histone deacetylase 1 (*AtHDT1*) expression. *Genetics*, **165**, 399–409.
- Torres, M.A., Dangl, J.L. & Jones, J.D. (2002) Arabidopsis gp91phox homologues AtrbohD and AtrbohF are required for accumulation of reactive oxygen intermediates in the plant defense response. *Proceedings of the National Academy of Sciences of the United States of America*, **99**, 517–522.
- Ueda, M., Matsui, A., Nakamura, T., Abe, T., Sunaoshi, Y., Shimada, H. et al. (2018) Versatility of HDA19-deficiency in increasing the tolerance of Arabidopsis to different environmental stresses. *Plant Signaling & Behavior*, **13**, e1475808.
- Ueda, M., Matsui, A., Tanaka, M., Nakamura, T., Abe, T., Sako, K. et al. (2017) The distinct roles of class I and II RPD3-like histone deacetylases in salinity stress response. *Plant Physiology*, **175**, 1760–1773.
- Vaahra, L., Brosché, M., Wrzaczek, M. & Kangasjärvi, J. (2014) Specificity in ROS signaling and transcript signatures. *Antioxidants & Redox Signaling*, **21**, 1422–1441.
- Wang, Y.-Q., Feechan, A., Yun, B.-W., Shafiei, R., Hofmann, A., Taylor, P. et al. (2009) S-nitrosylation of AtSABP3 antagonizes the expression of plant immunity. *Journal of Biological Chemistry*, **284**, 2131–2137.
- Wang, Z., Cao, H., Sun, Y., Li, X., Chen, F., Carles, A. et al. (2013) Arabidopsis paired amphipathic helix proteins SNL1 and SNL2 redundantly regulate primary seed dormancy via abscisic acid-ethylene antagonism mediated by histone deacetylation. *The Plant Cell*, **25**, 149–166.
- Willems, P., Van Breusegem, F. & Huang, J. (2021) Contemporary proteomic strategies for cysteine redoxome profiling. *Plant Physiology*, **186**, 110–124.
- Wrzaczek, M., Brosché, M. & Kangasjärvi, J. (2013) ROS signaling loops—production, perception, regulation. *Current Opinion in Plant Biology*, **16**, 575–582.
- Yang, H., Mu, J., Chen, L., Feng, J., Hu, J., Li, L. et al. (2015) S-nitrosylation positively regulates ascorbate peroxidase activity during plant stress responses. *Plant Physiology*, **167**, 1604–1615.
- Yruela Guerrero, I., Moreno-Yruela, C. & Olsen, C.A. (2021) Zn²⁺-dependent histone deacetylases in plants: structure and evolution. *Trends in Plant Science*, **26**, 741–757.

- Yuan, L., Liu, X., Luo, M., Yang, S. & Wu, K. (2013) Involvement of histone modifications in plant abiotic stress responses. *Journal of Integrative Plant Biology*, **55**, 892–901.
- Zhan, N., Wang, C., Chen, L., Yang, H., Feng, J., Gong, X. et al. (2018) S-nitrosylation targets GSNO reductase for selective autophagy during hypoxia responses in plants. *Molecular Cell*, **71**, 142–154.e6.
- Zheng, Y., Ge, J., Bao, C., Chang, W., Liu, J., Shao, J. et al. (2020) Histone deacetylase HDA9 and WRKY53 transcription factor are mutual antagonists in regulation of plant stress response. *Molecular Plant*, **13**, 598–611.
- Zhou, C., Zhang, L., Duan, J., Miki, B. & Wu, K. (2005) HISTONE DEACETYLASE19 is involved in Jasmonic acid and ethylene signaling of pathogen response in Arabidopsis. *The Plant Cell*, **17**, 1196–1204.
- Zhou, Y., Tan, B., Luo, M., Li, Y., Liu, C., Chen, C. et al. (2013) HISTONE DEACETYLASE19 interacts with HSL1 and participates in the repression of seed maturation genes in Arabidopsis seedlings. *The Plant Cell*, **25**, 134–148.